LAPPEENRANTA UNIVERSITY OF TECHNOLOGY
LUT School of Energy Systems
LUT Mechanical Engineering

Teemu Priha

HARD OBJECT DETECTION INSIDE SOIL WITH HAPTIC SENSING IN EXCAVATOR CONTROL

Examiners: Professor Heikki Handroos
D. Sc. (Tech) Lauri Luostarinen

TIIVISTELMÄ

Lappeenrannan Teknillinen yliopisto
LUT School of Energy Systems
LUT Kone

Teemu Priha

Hard object detection inside soil with haptic sensing in excavator control

Diplomityö

2017

57 sivua, 22 kuvaa, 4 taulukkoa ja 1 liite

Tarkastajat: Professori Heikki Handroos
TkT Lauri Luostarinen

Hakusanat: kaivinkone, kauko-ohjaus, haptinen ohjaus, simulointi

Nykyisten kauko-ohjattavien maansiirtokoneiden ongelmana on täydellinen fyysisen palautteen puute, jota koneen kuljettaja normaalisti hyödyntäisi työskennellessään koneen ohjaamosta käsin. Tämä voi johtaa ongelmiin ja aiheuttaa niin konkreettista kuin taloudellista vahinkoa kauhan osuessa maaperässä mahdollisesti oleviin kiinteisiin esteisiin, kuten lohkareisiin, putkiin tai sähköjohtoihin. Tämän työn tarkoituksena on tutkia yhtä mahdollista ratkaisua kyseiseen ongelmaan kehittämällä ohjausjärjestelmä, joka ensin tunnistaa kauhan osuman maaperässä piilossa olevaan esteeseen, sekä antaa kuljettajalle välittömästi haptisen palautteen tärisevän ohjaussauvan avulla. Ohjausjärjestelmän toimivuutta testataan reaaliaikaisessa simulaatioympäristössä.

Työ on jaettu kahteen osioon siten, että olemassa olevaa tutkimustietoa kerätään kirjallisuuskatsauksen avulla, jonka jälkeen haptinen ohjausjärjestelmä kehitetään toimimaan yhteistyössä Mevean tuottamalla reaaliaikaiseen simulaatioon perustuvalla alustalla. Esteentunnistus perustuu laskennalliseen menetelmään, jossa kaivurin puomin niveliin kohdistuvan väännön perusteella kyetään havaitsemaan epänormaalin suuret kaivurin kauhaan kohdistuvat voimat. Havaitessaan osuman, järjestelmä tuottaa tärinäsignaalin, joka lähetetään ohjaussauvaan integroituun tärinämoottoriin tuottaen kuljettajalle tiedon esteeseen osumisesta.

Työn tuloksena syntyi katsaus olemassa olevaan tutkimustietoon liittyen työkoneiden kauko-ohjaukseen sekä haptisen palautteen käyttämiseen vastaavissa sovelluksissa. Sen lisäksi haptisen palautteen tutkintaan kehitettiin kokeellinen järjestelmä reaaliaikaiseen simulaatiomalliin luodussa ympäristössä. Järjestelmä mahdollistaa jatkossa lisäkehityksen ja tutkimuksen simulaatioympäristössä, sekä vastaavan ohjausjärjestelmän implementoinnin tosimaailmaan.

ABSTRACT

Lappeenranta University of Technology
LUT School of Energy Systems
LUT Mechanical Engineering

Teemu Priha

Hard object detection inside soil with haptic sensing in excavator control

Master's thesis

2017

57 pages, 22 figures, 4 tables and 1 appendice

Examiners: Professor Heikki Handroos
D. Sc (Tech) Lauri Luostarinen

Keywords: excavator, haptics, force feedback, teleoperation, object detection, simulation

The problem with currently available remote-control systems for excavators is the completely non-existent operator feedback of forces affecting the excavator bucket during digging operations. This leads to problems in detecting underground obstacles like wires or water pipes, which could lead to costly damages. One possible solution for this problem is examined in this thesis by developing and studying a haptic control system for a simulation model of a remote-controlled excavator.

First, a literature review was conducted to establish a picture of previous research on the subject. The simulation model was created and run in real-time using Mevea Simulation software. A method based on calculating the torques on the joints of the excavator arm was used to determine the forces affecting the excavator bucket, with a finite impulse response filter utilized to screen out the dynamic forces in the system. The resulting force signal was then used to actuate an electric vibration motor embedded into a general-purpose mobile working machine joystick.

As a result of this work, a picture of haptic system research for earth moving machines was established. In addition, a control system for testing the haptic feedback was created and studied utilising real-time simulation. This system can be used for further studies on the subject, and the object detection system could be implemented to a real-world excavator.

ACKNOWLEDGEMENTS

The creation of this study wouldn't have been possible without the invaluable support and advice I've been given by the examiners, teachers and the office personnel at LUT. First, I would like to thank professor Heikki Handroos for giving me the opportunity to work on this thesis and his guidance throughout the process. I also highly appreciate the help Lauri Luostarinen has given me, both in practical matters as well as theoretical ones. To my parents, who have given me their unconditional support throughout the years, thank you.

Teemu Priha
Lappeenranta 27.10.2017

TABLE OF CONTENTS

LIST OF SYMBOLS AND ABBREVIATIONS

a	Area of flow
A_{p}	Piston area
A_{r}	Piston area on rod-side
a_3	Distance between points *F* and O_2
b	Width of the cut soil
B_{ei}	Effective bulk modulus of hydraulic fluid (including dissolved air) and its container
b_3	Distance between points I and O_2
c	Soil cohesion
d	Length
d	Depth of the bucket relative to soil
e_1	Distance between points P and O_3
e_2	Distance between points P and K
e_3	Distance between points K and L
e_4	Distance between points L and O_3
$\boldsymbol{C}$	Vector of kinematic constraint equations
$\boldsymbol{C}_{\boldsymbol{q}^i}$	Constraint Jacobian matrix
$\boldsymbol{C}_{\boldsymbol{q}_t}$	First time derivative of Jacobian constraint matrix
$\boldsymbol{C}_{tt}$	Second time derivative of the kinematic vector of constraint
C_{v}	Flow coefficient
$\boldsymbol{C}_{\mathbf{z}}$	Constraint Jacobian matrix
c_{23}	$\cos(\theta_2+\theta_3)$
F	Force
f	Force
F_r	Soil force on the bucket, parallel to digging direction
F_μ	Friction force between the piston and the cylinder wall
F_3	Dipper arm cylinder force
F_4	Bucket cylinder force
G_3	Gravitational force affecting the dipper arm

G_4	Gravitational force affecting the bucket
h	Thickness of cut soil
h	Distance between points J and L
k_p, k_s	Specific cutting resistances for silty clay
k_1	Distance between points L and P
k_2	Distance between points K and O_3
L_{JO3}	Distance between points J and O_3
L_{O2G3}	Distance between points O_2 and G_3
L_{O3G4}	Distance between points O_3 and G_4
l_3	Length between points O_2 and O_3
L_4	Bucket cylinder length
$\boldsymbol{M}^i$	Symmetric mass matrix
m_3	Mass of the dipper arm
m_4	Mass of the bucket
N	Pressure force applied by the bucket on the soil
N_γ	Factor for frictional strength of the soil
N_C	Factor for geometry of the bucket
N_q	Factor for relative strength properties of the bucket and the soil
$\dot{p}_i$	Change of pressure of volume *i* with respect to time
p_1	Cylinder pressure on the piston side
p_2	Cylinder pressure on the rod-side
q	Vertical pressure from the bucket onto the surface of the soil
$\boldsymbol{Q}_d$	Vector of quadratic velocity terms
$\boldsymbol{Q}_e^i$	Vector of generalized forces applied on a body
$Q_{i,i}$	Flow rate into volume *i*
Q_L	Internal leakage flow rate
$Q_{o,i}$	Flow rate out of volume *i*
$\boldsymbol{Q}_v^i$	Quadratic velocity vector
$\boldsymbol{q}^i$	Vector of generalized coordinates
$\ddot{\boldsymbol{q}}^i$	Vector of acceleration
Q_1	Volume flow to the piston side of a cylinder

Q_2	Volume flow to the rod-side of a cylinder
R	Velocity transformation matrix
t	Time
v	Piston speed
v_b	Volume of the bucket
V_i	Capacity of volume *i*
$\dot{V}_i$	Change of capacity in volume *i* with respect to time
v_s	Volume of the dug soil
w	Width of the bucket
x	Displacement
Δx_i	Horizontal increment in meters
z	Relative coordinates
$\ddot{\mathbf{z}}$	Relative joint accelerations
α	Matrix for penalty terms
α	$\angle JO_3K$
β	$\angle LO_3J$
γ	Density of the soil
γ_1	$\angle LKP$
γ_2	$\angle JKL$
γ_3	$\angle KPO_2$
γ_4	Bucket joint angle
δW_e^i	Virtual work of external forces acting on body *i*
δW_i^i	Virtual work of the inertia forces acting on body *i*
ε	Resistance coefficient of the soil when filling the bucket
θ	Angle
$\boldsymbol{\theta}_2$	Boom joint angle from Mevea
$\boldsymbol{\theta}_3$	Dipper joint angle from Mevea
$\boldsymbol{\theta}_4$	Bucket joint angle from Mevea
θ_{234}	Sum of angles θ_2, θ_3 and θ_4
$\boldsymbol{\lambda}$	Vector of Lagrange multipliers
$\boldsymbol{\lambda}^*$	Vector of penalty forces

$\boldsymbol{\lambda_i^*}$	Unknown multipliers
μ	Friction coefficient between the excavator bucket and soil
$\boldsymbol{\mu}$	Matrix for constraint damping ratios
ρ	Density of fluid
σ_4	Angle between points G_4, O_3 and O_4
σ_5	Angle between points G_3, O_2 and O_3
$\boldsymbol{\tau_d}$	System torque
$\boldsymbol{\tau_l}$	Load torque
$\boldsymbol{\tau_s}$	Total torque
τ_3	Dipper arm joint torque
τ_4	Bucket joint torque
$\boldsymbol{\Omega}$	Matrix for natural frequencies

DOF	Degrees of freedom
FEE	Fundamental earthmoving equation
FEM	Finite element method
FIR	Finite impulse response
HILS	Hardware-in-the-loop-simulation
MANET	Mobile Ad-Hoc Network
OBB	Oriented bounding boxes
VE	Virtual environment
WNCS	Wireless networked control system

1 INTRODUCTION

Traditionally the use of simulation in product development has been limited to time consuming and calculationally heavy methods like finite element method (FEM), which might require hours of processing in order to analyse only a few seconds of real life events. Thus, this so called offline simulation has some limitations when analysis of a complete machine system is required. Real-time simulation offers the possibility to construct a virtual prototype of the whole system including the operator, control system, machine and the operating environment. Additionally, it allows the testing of a control system and the machine before the need of real life prototyping as well as machine testing from the operator's point of view.

Machine teleoperation is mainly needed when working in a hazardous environment like a nuclear disaster or combat zone. It could also allow the operators to work with a fleet of machines from a centralized location. Adding the teleoperation functionality has been possible for a while, but has not gained popularity on a larger scale. This is partly due to the fact that certain amount of feedback is required by the machine operator in order to achieve a comparable amount of precision to a traditional machine.

Haptic control systems have been developed to recreate the feeling of using direct controllers by providing forces or vibrations to the user in order to improve the usability and productivity of teleoperation systems. Current teleoperation systems are lacking in feedback when comparing to directly operated systems, which coincidentally results in the need of having a person at the operating site to spot objects like large rocks, electrical wires or water pipes, which might be damaged or cause damage to the machine if the operator can't feel the increase in digging force caused by obstacles.

1.1 Objective of this work

The overall aim of this paper is to study the possibility of controlling an excavator via haptic feedback system. The work is split into two main sections: a literature review and an experimental part. The purpose of the literature review is to examine the existing technology related to teleoperation and haptic control of working machines, or the combination of both. In the experimental part, a solution to accurately represent the forces affecting the excavator bucket to the machine operator using a haptic feedback system is proposed and compared to a traditional control system without haptic feedback.

The goal of this paper is to answer the following questions:

- What is the current state of teleoperated and haptic controlled work machines?
- Can the detection of hidden underground obstacles be improved by utilizing a haptic feedback system in a real-time simulation environment?

2 LITERATURE REVIEW

Mobile working machines are used extensively around the globe to perform various construction tasks like earthmoving, levelling, as well as demolition. An excavator is a typical mobile working machine. In most cases, they are powered by a diesel engine, equipped with hydraulic actuators, and operated by a human. Similar machinery can also be found in forestry, mining, as well as agricultural industry.

In some scenarios, however, manned human operation of the machine can be difficult or dangerous to the operator. Such scenarios include nuclear disasters, earthquakes, volcanic eruptions (Hiramatsu, Aono & Nishio 2002, p. 505) or working on a combat zone. In these conditions, it would be safer for the machine to be unmanned, namely autonomous or remote controlled. Autonomous operation would require considerably more development at its current standing (Schmidt & Karsten 2010, p. 825). The amount and complexity of information needed to operate an excavator autonomously is difficult to process, and the control algorithms must be highly sophisticated to cope with different tasks and environments. Teleoperation, however, could be implemented with relative ease to existing excavator equipment. Thus, much of the research has been directed to teleoperation and haptic feedback systems. A review of articles published from 2000 to present date related to teleoperation, haptics, and the combination of both is carried out in the following chapters.

2.1 Teleoperation

The definition of teleoperation per Oxford Dictionary, is “The control of a device or machine remotely.” Teleoperation therefore includes wired as well as wireless data transfer. Wired teleoperation limits the area of operation to the length of the connecting cables. Cables would also be subject to harsh conditions, making their durability uncertain. Thus, this paper will focus on wireless teleoperation of excavators.

2.1.1 Teleoperation of excavators

As noted before, teleoperation has been favoured over autonomous excavator studies due to the complex control algorithms and sensor arrays required for autonomous operation. One additional reason has been studied and presented by Sakaida et al. (2006). The authors noted that a skilful excavator operator can achieve higher efficiency during a digging task than a non-

skilful one. To make autonomous excavator operation as efficient as human operated machine, it would require either self-learning capability or every operational scenario of excavator usage would have to be copied from a skilful operator.

Some of the earliest experiments regarding teleoperated excavators was conducted by Burks, Killough, Thompson and Rossi (1994), whose study focused on evaluating the feasibility of unexploded ordnance removal by remote operated backhoe installed on a Mercedes-Benz Unimog truck (Figure 1). The proposed system includes a control panel equipped with three monitors, two joysticks for backhoe control, separate joysticks for camera controls, as well as a trackball and several buttons for miscellaneous controls. Although the communication between the vehicle and the control system was designed to be carried out by microwave radio for video channels and Ethernet radio for data transfer, the demonstrated system utilised a coaxial cable for all communications. Three cameras in total were mounted on the vehicle, two of which were located behind the cabin providing a general view of the working area, and one mounted on the backhoe boom which proved to be highly beneficial by allowing the operator to closely observe into the bucket and the digging area. (Burks et al. 1994, p. 7.)

The feedback for the operator was mainly implemented via the graphical user interface on the three monitors. In addition to video feedback, the monitors provide an animated graphic of the backhoe and the working area from top down as well as from the side, giving the operator an improved perception of depth. By using various sensors installed on the backhoe, the side view can be used to present the joint angles and therefore the position of the backhoe links. The ground level is also presented in 1 feet (0.3048 m) increments allowing for improved bucket positioning during digging. Perhaps the most interesting detail in the system is the torque indicators included in the side view. Instead of haptic feedback, the loss of feel compared to a manned excavator is compensated by a pie chart located on each joint in the side view. The torque limit was preset so that the operator is given an audiovisual warning by changing the colour of the pie from grey to red and giving a beeping alarm sound when the torque would be high enough to lift or move the vehicle. (Burks et al. 1994, p. 12-13.)

Figure 1. Teleoperated excavation vehicle pictured during waste retrieval demonstration. Note the two cameras visible behind the cabin. (Burks et al. 1994, p. 5.)

Although teleoperated machinery has yet to see extensive commercial usage, some usage has been experimented in real-life situations. In March 2000, a volcanic eruption occurred in Mt. Usuzan, Japan, creating destructive, hot mudflows. Several unmanned vehicles were deployed to begin restoration of damaged areas and structures, and to prevent a secondary disaster from possible subsequent eruptions. Unmanned and remotely controlled bulldozers, dump trucks, hydraulic shovels and assisting mobile camera vehicles were successfully utilized during the operation. The vehicles were equipped with cameras and radio transmission equipment to enable controllability from a remote location (Figure 2). Also, an autonomous and unmanned helicopter was used to scout the area for the most critical areas before beginning the restoration work. A maximum distance of 1.2 km was reached in remote operation, even though the radio signal was interfered by various physical obstacles. 16 temporary mobile radio stations were constructed to provide required coverage of the area. 424 MHz radio signal was used to transmit the control signal, whereas 2.4 GHz band was utilized for video transmission. (Hiramatsu et al. 2002, p. 505-507.)

Although the operation was finished successfully, some difficulties were identified. The radio systems suffered some damage from cinders and additional mud eruptions. Additionally, the

work was hindered and sometimes completely halted by poor visibility due to snowstorms, as well as continuing volcanic eruptions. Also, the recognition of working areas and travel routes was noted to be impossible at certain locations. (Hiramatsu et al. 2002, p. 508.)

Figure 2. Machine operators in a remote-control room (Hiramatsu et al. 2002, p. 506).

In a more recent study by Yang et al. (2008) a remote-control system equipped with two joysticks and a notebook computer was proposed (Figure 3). The exact details of the used teleoperation technology are not disclosed, but the joystick signals are said to be transmitted via radio frequency signal, whereas the notebook is connected using inbuilt wireless LAN adapter. Thus, the operational range of teleoperation can be expected to be relatively restricted.

Figure 3. Remote-control station equipped with two electronic joysticks and a notebook PC (Yang, Jin & Kwon 2008, p. 443).

Yu, Liu & Hasan (2010) focused on modeling, communication and control of a teleoperated excavator. The proposed system (Figure 4) is based on Mobile Ad-Hoc Network (MANET), which is an autonomous network of mobile devices, each with the ability to route network traffic among other devices on the same network (Tavli & Heinzelman 2006, p. 2). The use of MANET allows the teleoperation system to function independently from existing networks, enabling operation in areas with poor or non-existent network infrastructure. The relay robots could also be equipped with additional cameras to provide improved video feedback from the work site.

In total, 11 key factors for developing an autonomous remotely controllable excavator were identified (Figure 5). Since autonomous operation is out of scope of this paper, only issues related to teleoperation are presented. The first of the proposed factors are sensors and cameras. Required sensors for teleoperation include position and velocity sensors to monitor the angles and velocities of the joints. Force sensors are needed to measure the forces between the bucket of the excavator and the environment. Also, vibration sensors should be utilized to sense undesirable vibrations in the excavator. Furthermore, cameras can be considered as sensors as well, providing the operator with important visual information. Cameras can be installed on the excavator itself, as well as the assisting observer robots providing various viewing angles improving the operators view of the working area. (Yu, Liu & Hasan 2010, p. 70.)

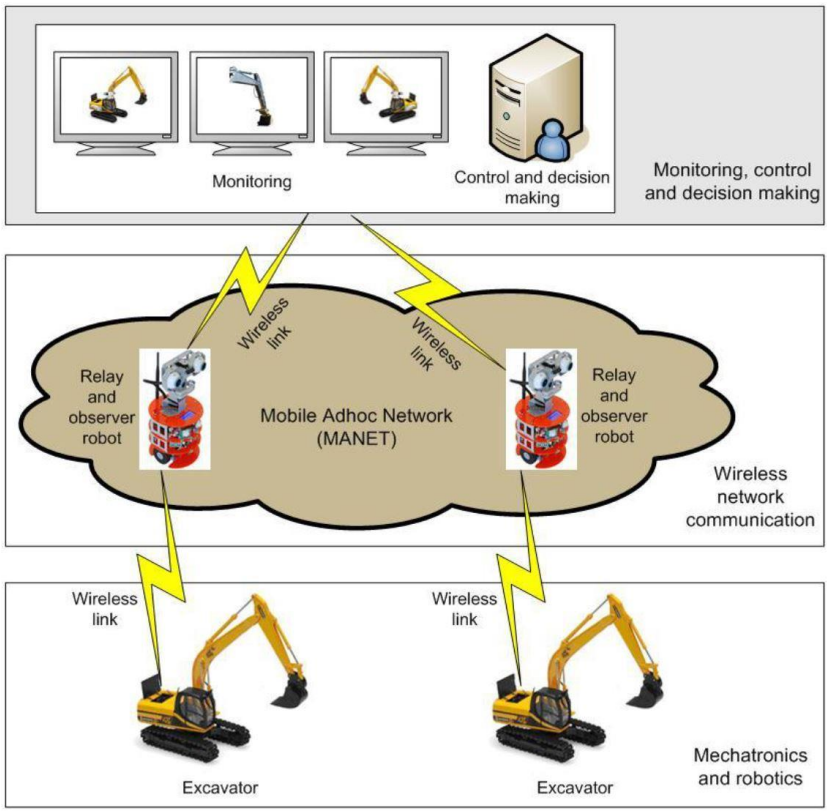

Figure 4. Excavator teleoperation system design (Yu, Liu & Hasan 2010, p. 70).

Next, the hydraulic actuators of the excavator need to be studied in order to determine the nonlinear dynamics of the hydraulic system. Friction in the hydraulic cylinders, and the flow characteristics of hydraulic fluid through orifices and valve spools have the most notable effect. (Yu, Liu & Hasan 2010, p. 71.)

The MANET remote control system is proposed to be realized using IEEE 802.11 standards, which are described as low cost and easily deployable. Modern wireless networks provide enough bandwidth to simultaneously carry live video feed as well as sensor and actuator data. The wireless signals will be corrupted by unwanted noise however, which need to be eliminated by using filters in signal processing. If the bandwidth and processing power are sufficient, even a virtual 3D view of the excavator surroundings can be created. (Yu, Liu & Hasan 2010, p. 71.)

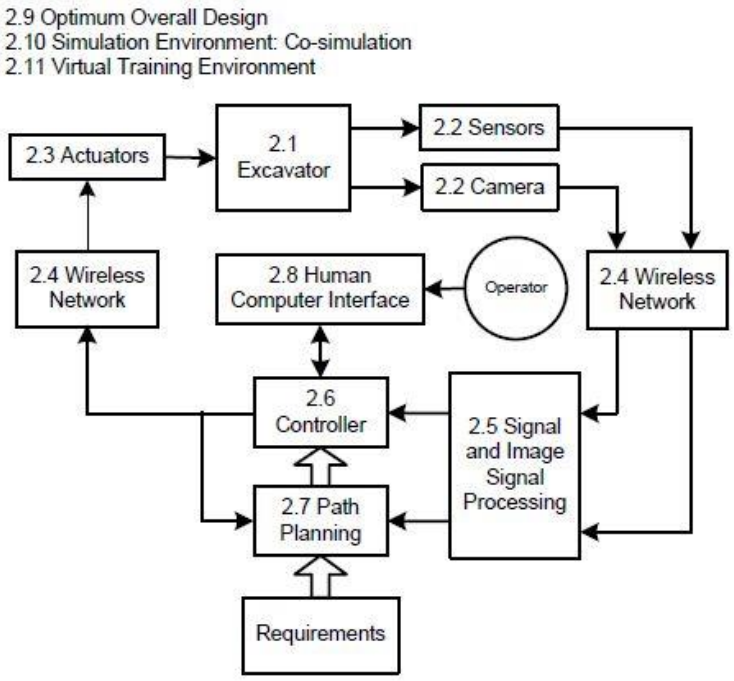

Figure 5. Schematic of the proposed architecture of the teleoperation system (Yu, Liu & Hasan 2010, p. 72).

The research of MANET and other wireless networked control systems (WNCS) is mainly based on work done in simulation environment due to the cost and time required by research in real setting. Various tools for simulating wireless network exist, and are presented in Table 1 including their strengths and weaknesses. The main software utilized in most cases is MATLAB, and the graphical programming environment Simulink.

Table 1. Network simulation tools (Yu, Liu & Hasan 2010, p. 76).

Name	**Developer**	**+**	**-**	**Remarks**
Optimised Network Engineering Tool (OPNET)	OPNET Technologies, Inc.	Most detailed network simulation	Commercial	Acquired by Riverbed Technology in 2012
Network Simulator version 2 (ns-2)	Open source	Free (GPLv2)	Lacking necessary parameters for MANET simulation	Replaced by ns-3
TrueTime	Cervin et al. (2003)	MATLAB integration Free (GPL)		TrueTime 2.0 released in 2016

2.2 Haptics

The field of haptics is wide and includes several applications and disciplines. To better understand the haptic control of excavators, the following chapter is used to provide background knowledge of related haptic systems in general.

2.2.1 Introduction to haptics

Originating from the Greek verb “hapto”, meaning “to touch”, the word haptic refers to the ability to touch and feel objects. According to Samur (2012, p. 3), “A haptic interface is an actuated, computer controlled and instrumented device that allows a human user to touch and manipulate objects either within a virtual environment (VE) -- or in a real world through a slave of a teleoperated systems such as for surgical robotics.”. Unlike traditional control schemes which only provide an input interface, haptic systems are also capable of creating outputs that are used to give feedback to the operator. Therefore, haptic feedback allows the use of mechanical energy as information between a VE or remote location and the operator, even without a mechanical link. (Mihelj & Podobnik 2012, p. 35.)

The most distinguishing feature of haptic control systems is the bilateral (sometimes referred as bidirectional) nature of data transfer, whereas systems without feedback merely operate unilaterally. As can be seen from Figure 6, the operator controls the movement (velocity) of the slave system via the haptic interface, while at the same time receiving information of the direction and the amount of force affecting the slave system. Hence, it becomes vital to measure (teleoperation) or compute (VE) the forces which are created in the slave system as a consequence of operator inputs. (Mihelj & Podobnik 2012, p. 36.)

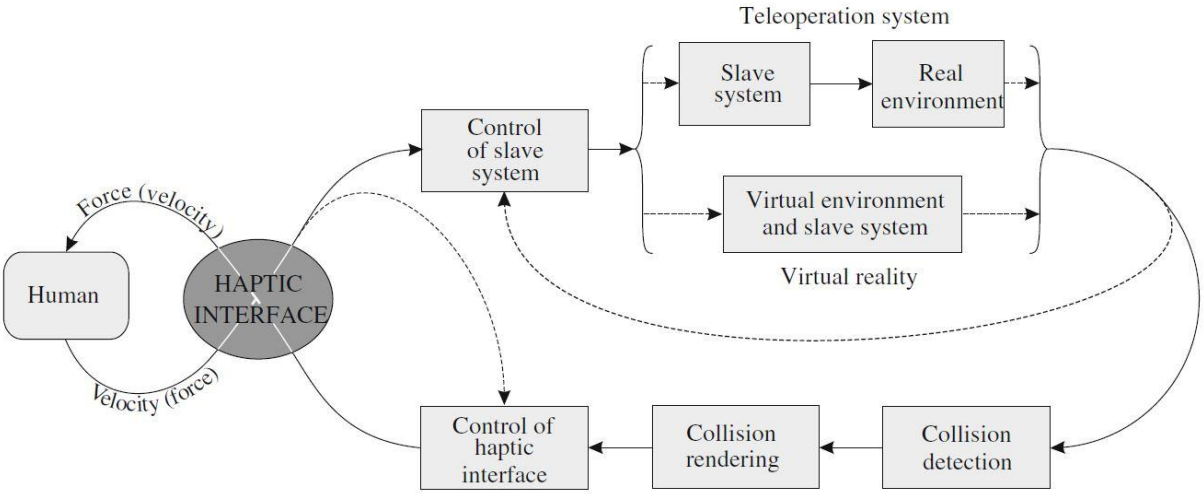

Figure 6. A schematic view of haptic interaction between human operator and either a teleoperated or virtual slave system (Mihelj & Podobnik 2012, p. 37).

2.2.2 Haptic control of excavators

Currently haptic feedback is mainly studied in conjunction with teleoperation systems. The main motivation behind haptic control system research is the need to improve operator feedback in remote control scenarios, where the machine operator is relying on video signal to control the excavator. During manned operation, the driver can sense the movements and forces of the excavator from not only audio-visual cues, but via tactile feedback as well. Implementing a haptic feedback system to a teleoperated excavator could improve the precision and efficiency of the excavator.

In the journal paper by Yun-Joo & Myeong-Kwan (2015), the authors studied the performance of a virtual excavator controlled with one joystick capable of delivering haptic feedback. The studied system, shown in Figure 7, included three physical hydraulic cylinders creating a hardware-in-the-loop-simulation (HILS). The use of physical hydraulic cylinders is reasoned by the difficulties related to the simulation of hydraulic systems, namely the valve orifice effect and the compressibility of the hydraulic oil. Furthermore, external loads can be effectively applied on the utilized hydraulic cylinder setup.

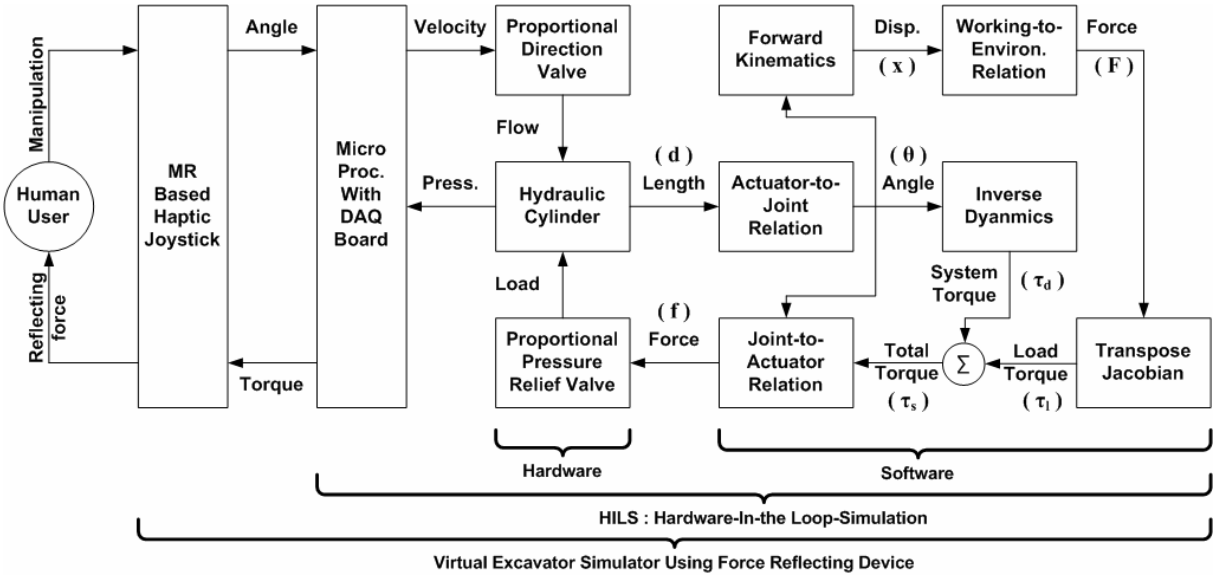

Figure 7. Schematic view of the studied setup including haptic joystick, hydraulic cylinders and the simulation software (Yun-Joo & Myeong-Kwan 2015, p. 398).

Furthermore, Osafo-Yeaboah et al. (2010) studied the usability of haptic excavator control in a simulation environment. The studied setup comprised of Phantom Premium 1.0A haptic input device installed in a stationary Bobcat excavator cabin. Connected by a local area network, three computers in total were required. One computer was used to control the Phantom device, one was connected to a 52" LCD screen providing the operator with graphical feedback from the simulation environment, and a third computer was utilized to execute the bespoke dynamics simulation, developed with C++ and MATLAB programming. Twenty students from Georgia Institute of technology were recruited as test operators with no prior experience of operating an excavator. (Osafo-Yeaboah et al. 2010, p. 3.)

Several problems related to usability were identified during the study, most notably the lack of feeling of collision between the bucket and obstacles. Also, multiple problems related to the efficiency and flexibility of the Phantom interface were recognized, such as poor synchronization between the stylus and the bucket, inability to maintain steady control of the excavator and difficulties in maintaining hand-eye coordination during operation. Nevertheless, the authors in Osafo-Yeaboah et al. (2010) stated the user interface was "intuitive, easy to learn and easy to use", thus potentially cutting the time needed for new excavator operators to learn the controls. It is also noted that the haptic control scheme could reduce costs of the training period and furthermore during work tasks by improving efficiency by making the operators better aware of underground obstacles. (Osafo-Yeaboah et al. 2010, pp. 5-6.)

2.3 Combination of teleoperation and haptic control scheme

When compared to a traditional manned control system, the efficiency of teleoperation is said to be 60-70% of that (Ban 2002, p. 243). Since the main drawback of teleoperation compared to manned control of excavator is the working efficiency, haptic control schemes have been studied and developed to improve the performance of teleoperated machines. In a study by Hayashi & Tamura (2009), the authors studied tactile feedback as means to improve the efficiency of excavator teleoperation. The experimental setup consisted of a common excavator model, equipped with a laser range finding sensor (JENOPTIK LDM301.100) on the bucket used to determine the distance to the ground. Based on preliminary tests, a vibrator attached to the operator's right hand was set to power on 150ms before presumed ground contact, calculated from bucket velocity and distance to ground. The control and video signals between the excavator and control room were carried via LAN cable. (Hayashi & Tamura 2009, p. 2761.)

The experiment included two different tasks, where the operator had to move the bucket from various starting positions to a fixed target position. Each task was carried out utilizing manned operation, teleoperation, and teleoperation with haptics. One experienced operator was employed to operate the machine for all the tests. The study concluded that the movement time from start to finish was reduced with tactile feedback. Additionally, it was noted that the movement time was dependent on the distance between the ground and the bucket as seen from the monitor, as opposed to the actual distance (Figure 8). (Hayashi & Tamura 2009, p. 2764.)

Figure 8. The distance between ground and the bucket as seen from the camera on the excavator. Actual distance to ground was 2.24 m (left) and 4.47 m (right). (Hayashi & Tamura 2009, p. 2763.)

3 SIMULATION ENVIRONMENT

The simulation environment utilized in this thesis was solely Mevea Software, developed by Mevea Ltd. The software provides a real-time simulation environment as well as tools to create and edit virtual machine models. It also offers connectivity to peripheral devices, including motion platforms, joysticks and various other I/O-devices, as well as software such as Simulink. In the following chapters, some of the functionality and details related to the simulation environment are presented in further detail.

3.1 Multibody system dynamics

To understand the operating principle of Mevea, one needs to have knowledge of dynamics of multibody systems. Multibody system dynamics is an area of study related to analysing mechanical and physical systems, such as various machines, vehicles, robotics, and space structures. These multibody systems consist rigid and deformable bodies which can have relative translational and rotational movement. As seen in Figure 9, the different bodies are connected by different types of joints and force elements, making the system kinematically constrained. Multibody systems are most often exceedingly nonlinear in nature, and solving the dynamics of such systems has only become viable in the recent decades after the increase in computational calculation power. The motivation for research in the area of multibody dynamics has been driven by the interest in simulation and design of complex, large scale systems where development costs are usually highest. Also, the increase in computing power allows the accuracy of the analysis to be improved by implementing additional factors to the simulation, such as deformation and collision properties. (Shabana 1998, p. 1-3.)

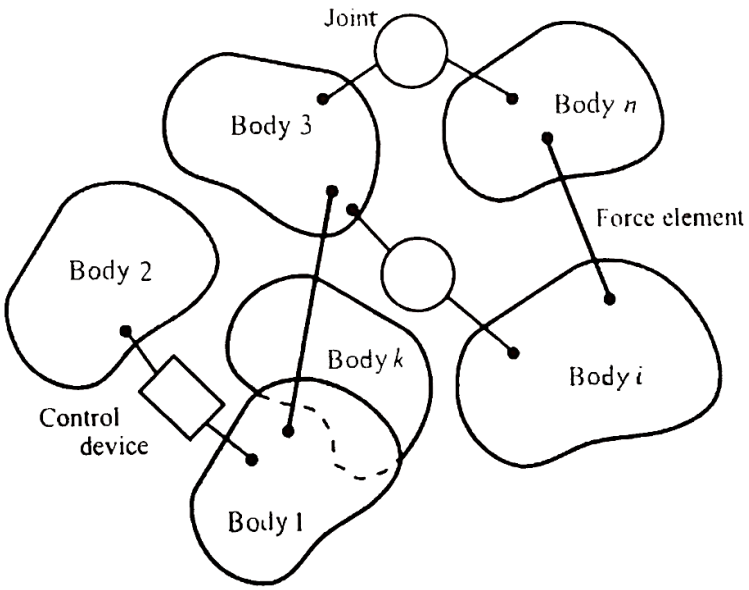

Figure 9. Multibody system (Shabana 1998, p. 3).

Several different methods have been developed to solve the multibody system dynamics, such as the iterative Newton-Rhapson method (Shabana 2010, p. 144), and Baumgarte's constraint stabilization method (Shabana 2010, p. 347). However, Mevea utilizes three main methods for solving the multibody system dynamics of rigid bodies, namely the Lagrange multiplier method, the augmented Lagrangian method, and the recursive method. In addition, the behaviour of flexible bodies in the simulation is solved by using the floating frame of reference approach. The basics of these methods are presented in the following chapters. (Korkealaakso 2015, p. 8.)

3.1.1 Lagrange multiplier method

The Lagrange multiplier method is based on the equations of motion, developed from the principle of virtual work for unconstrained motion. Virtual work by inertial forces equals virtual work of the forces acting on a rigid body *i*, and can be written as

$$\delta W_i^i = \delta W_e^i \tag{1}$$

where δW_i^i is the virtual work of the inertia forces, and δW_e^i is the virtual work of external forces. The virtual work of inertia on a rigid body is

$$\delta W_i^i = [\boldsymbol{M}^i \ddot{\boldsymbol{q}}^i - \boldsymbol{Q}_v^i]^T \cdot \delta \boldsymbol{q}^i \tag{2}$$

where $\boldsymbol{M}^i$ is the symmetric mass matrix, $\ddot{\boldsymbol{q}}^i$ is the acceleration vector, $\boldsymbol{Q}_v^i$ is the quadratic velocity vector, and $\boldsymbol{q}^i$ is the vector of generalized coordinates. Furthermore, the work done by external forces can be written as

$$\delta W_e^i = {\boldsymbol{Q}_e^i}^T \cdot \delta \boldsymbol{q}^i \tag{3}$$

where $\boldsymbol{Q}_e^i$ is the vector of generalized forces applied on the body. When inserting equations 2 and 3 into equation 1, we get:

$$[\boldsymbol{M}^i \ddot{\boldsymbol{q}}^i - \boldsymbol{Q}_v^i - \boldsymbol{Q}_e^i]^T \cdot \delta \boldsymbol{q}^i = 0 \tag{4}$$

Since this solution only applies to unconstrained motion, the Lagrange multiplier method is utilized to build the dynamic equations for constrained multibody systems. Specifically, the term $[\boldsymbol{M}^i \ddot{\boldsymbol{q}}^i - \boldsymbol{Q}_v^i - \boldsymbol{Q}_e^i]$ needs to be set equal to zero, which can be achieved by inserting the Lagrange multipliers into equation 4, while at the same time satisfying the following condition (Shabana 2010, p. 408):

$$\boldsymbol{C}(\boldsymbol{q}, t) = 0 \tag{5}$$

where $\boldsymbol{C}$ is the vector of kinematic constraint equations and t is time. The Lagrange multipliers allow the computationally efficient calculation of constraint forces by augmenting constraint equations into the equations of motion (Shabana 2010, p. 405). Lagrange multipliers consist of vector $\boldsymbol{\lambda}$, which is equal in dimension to the number of constraint equations (Shabana 2010, p. 312). Introducing the Lagrange multipliers into equation 4 we get

$$\boldsymbol{M}^i \ddot{\boldsymbol{q}}^i - \boldsymbol{Q}_v^i - \boldsymbol{Q}_e^i + \boldsymbol{C}_{\boldsymbol{q}^i}^T \boldsymbol{\lambda} = 0 \tag{6}$$

where $\boldsymbol{C}_{\boldsymbol{q}^i}$ is the constraint Jacobian matrix and $\boldsymbol{\lambda}$ is the vector of Lagrange multipliers. Finally, the equations can be combined to acquire a numerically solvable matrix form (Shabana 2010, p. 407):

$$\begin{bmatrix} \ddot{\boldsymbol{q}} \\ \boldsymbol{\lambda} \end{bmatrix} = \begin{bmatrix} \boldsymbol{M} & \boldsymbol{C}_q^T \\ \boldsymbol{C}_{\boldsymbol{q}} & 0 \end{bmatrix}^{-1} \begin{bmatrix} \boldsymbol{Q}_e + \boldsymbol{Q}_v \\ \boldsymbol{Q}_d \end{bmatrix} \tag{7}$$

where $\boldsymbol{Q}_d$ is a vector which includes quadratic velocity terms. $\boldsymbol{Q}_d$ is acquired by differentiating the constraint equation 5 twice with respect to time, resulting in

$$\boldsymbol{Q}_d = -\boldsymbol{C}_{tt} - \left(\boldsymbol{C}_q \dot{\boldsymbol{q}}\right)_{\boldsymbol{q}} \dot{\boldsymbol{q}} - 2\boldsymbol{C}_{\boldsymbol{q}_t} \dot{\boldsymbol{q}} \tag{8}$$

where $\boldsymbol{C}_{\boldsymbol{q}_t}$is the first time derivative of Jacobian constraint matrix, and $\boldsymbol{C}_{tt}$ the second time derivative of the kinematic vector of constraint. (Shabana 2010, p. 406)

3.1.2 Augmented Lagrangian method

The augmented Lagrangian method was developed to negate problems related to penalty methods. When using penalty formulation, the user has to choose a penalty number used in calculation. Usually, a large penalty number is chosen to guarantee convergence, but this might produce large rounding errors and a high condition number. (Bayo, García de Jalón & Serna 1988, p. 188.)

The augmented Lagrangian method is then formulated as follows (Korkealaakso 2015, p. 8):

$$\begin{cases} \boldsymbol{M}\ddot{\boldsymbol{q}} + \boldsymbol{C}_{\boldsymbol{q}}^T \boldsymbol{\alpha}\left(\ddot{\boldsymbol{C}} + 2\boldsymbol{\Omega}\boldsymbol{\mu}\dot{\boldsymbol{C}} + \boldsymbol{\Omega}^2\boldsymbol{C}\right) + \boldsymbol{C}_{\boldsymbol{q}}^T \boldsymbol{\lambda}^* = \boldsymbol{Q}_{\boldsymbol{e}} + \boldsymbol{Q}_{\boldsymbol{v}} \\ \boldsymbol{\lambda} \cong \boldsymbol{\lambda}^* + \boldsymbol{\alpha}(\ddot{\boldsymbol{C}} + 2\boldsymbol{\Omega}\boldsymbol{\mu}\dot{\boldsymbol{C}} + \boldsymbol{\Omega}^2\boldsymbol{C}) \\ \boldsymbol{\lambda}_{i+1}^* = \boldsymbol{\lambda}_i^* - \boldsymbol{\alpha}(\ddot{\boldsymbol{C}} + 2\boldsymbol{\Omega}\boldsymbol{\mu}\dot{\boldsymbol{C}} + \boldsymbol{\Omega}^2\boldsymbol{C})_{i+1}\,, \quad i = 0,1,2,\ldots \end{cases} \tag{9}$$

where **α**, **Ω** and **μ** are matrices for, respectively, penalty terms, natural frequencies and constraint damping ratios. Additionally, $\boldsymbol{\lambda}^*$is the vector of penalty forces, and $\boldsymbol{\lambda}_{\boldsymbol{i}}^*$ are the unknown multipliers. To calculate the values of $\boldsymbol{\lambda}_{\boldsymbol{i}}^*$, an iterative process is implemented so that for the first iteration, $\boldsymbol{\lambda}_0^* = 0$. By using this improved method, a small penalty number can be used, therefore eliminating the problems with convergence and rounding errors. (Bayo et al. 1988, p. 187-191.)

3.1.3 Recursive method

Recursive methods have been developed to overcome the downside of augmented Lagrangian method and other augmented formulations. While the augmented Lagrangian method produces both differential and algebraic equations, recursive methods eliminate workless constraint forces, thus resulting in a simplistic group of differential equations. Therefore, computational effort for solving the equations is significantly reduced. When using the recursive method, the

equations of motion are formed with respect to joint degrees of freedom. Various methods for defining the recursive equations exist, but the resulting equations are always identical provided that matching joint variables are chosen. (Shabana 2010, p. 422-423.)

According to Korkealaakso (2015, p. 8) the recursive equations utilised in Mevea can be written as:

$$\begin{cases} (\boldsymbol{R}^T\boldsymbol{M}\boldsymbol{R} + \boldsymbol{\alpha}\boldsymbol{C}_{\boldsymbol{z}}^T\boldsymbol{C}_{\boldsymbol{z}})\ddot{\boldsymbol{z}} = \boldsymbol{R}^T(\boldsymbol{Q}_e + \boldsymbol{Q}_v) - \boldsymbol{R}^T\boldsymbol{M}\boldsymbol{S}_c + \boldsymbol{\alpha}\boldsymbol{C}_{\boldsymbol{z}}^T(\boldsymbol{Q}_c - \boldsymbol{C}_{\boldsymbol{q}}\boldsymbol{S}_{\boldsymbol{c}}) \\ \boldsymbol{C}_{\boldsymbol{z}} = \boldsymbol{C}_{\boldsymbol{q}}\boldsymbol{R} \end{cases} \quad (10)$$

where $\ddot{\mathbf{z}}$ is the relative joint accelerations, $\boldsymbol{C}_{\mathbf{z}}$ is the constraint Jacobian matrix with respect to the relative coordinates **z**, **R** is the velocity transformation matrix.

3.2 Software & hardware

The main software utilized during the preparation of the thesis was Mevea. Mevea software consists of several separate tools, but the two main modules are Mevea Modeller, and Mevea Solver. The Modeller is used to build and edit both the machine model, as well as the environment model. After the model is defined in the Modeller, it can be opened in the Solver tool. If the model was correctly built, it can be run and manipulated in the Solver in a realistic real time simulation. Furthermore, Simulink software was used in building the collision detection system for haptic sensing. The Simulink interface communicates with Mevea Solver via I/O -connection, similarly how a collision detection system would integrate into a real excavator control system. To ensure correct synchronization between the two programs, the Simulink model was run at 0.5 ms time step, whereas the Mevea Solver is working at 1 ms time step.

The body representing a sewer pipe was created using 3ds Max, which is a 3D modeling software created by Autodesk Inc., capable of various tasks related to 3D design. A generic sewer pipe design was created, with dimensions resembling a typical concrete sewer pipe (Rudus, 2017). The length of the pipe was chosen to be 3 m, which is approximately equal to the length of two sections of pipe. The diameter of the pipe was 30 cm. In order to import the part into the Mevea model, the pipe model was saved as .3DS-file.

Hardware used during the making of the thesis includes one PC running on 64-bit Windows 7 platform, equipped with two Intel Xeon E5-2630 CPUs and 32 GB of RAM. The mentioned PC is capable of running the real-time simulation and the Simulink model concurrently. Two joysticks were used to control the excavator model during simulation. A USB-connected joystick made by Thrustmaster was used for left handed controls, whereas a Penny & Giles Ltd. JC6000 joystick designed for off-highway vehicles was used for providing the haptic feedback (Figure 10). The JC6000 utilizes contactless Hall effect position sensors tracking the movement of the lever. Since the joystick isn't equipped for haptic feedback as standard, it was customized by installing one electric motor inside the handle to create vibration. Furthermore, the JC6000 can't be connected directly to a PC, so it was connected to the PC via USB-connected Arduino board. A separate C++ code was run on the board to decode the lever position as well as to activate the vibration motor in the joystick.

Figure 10. The Penny & Giles Ltd. JC6000 joystick installed on a testing rig along with the Arduino board.

Since the hydraulic system is an essential component of the excavator, the modeling of the hydraulic system is investigated in the next chapter.

3.3 Hydraulic model

The simulation of the hydraulic circuit is based on Pascal's Law of evenly distributed pressures (Korkealaakso 2015, p. 11), where the fluid pressure in one volume of the system is considered to be equal at every point when the fluid is not moving. The hydraulic circuit is separated into individual volumes by the components in the circuit. Figure 11 represents a basic hydraulic circuit, including (from the top) a hydraulic double acting cylinder, two check valves, a directional control valve, and hydraulic lines connecting the components to each other and to a hydraulic pump and tank. The components of the hydraulic system are mathematically modelled so that the flow rate of fluid into each separate volume is known. The flow rates are calculated utilising the equation of turbulent flow. Finally, a set of differential equations for the complete system is created allowing for dynamic analysis. (Durfee, Sun & Van de Ven 2015, p. 41.)

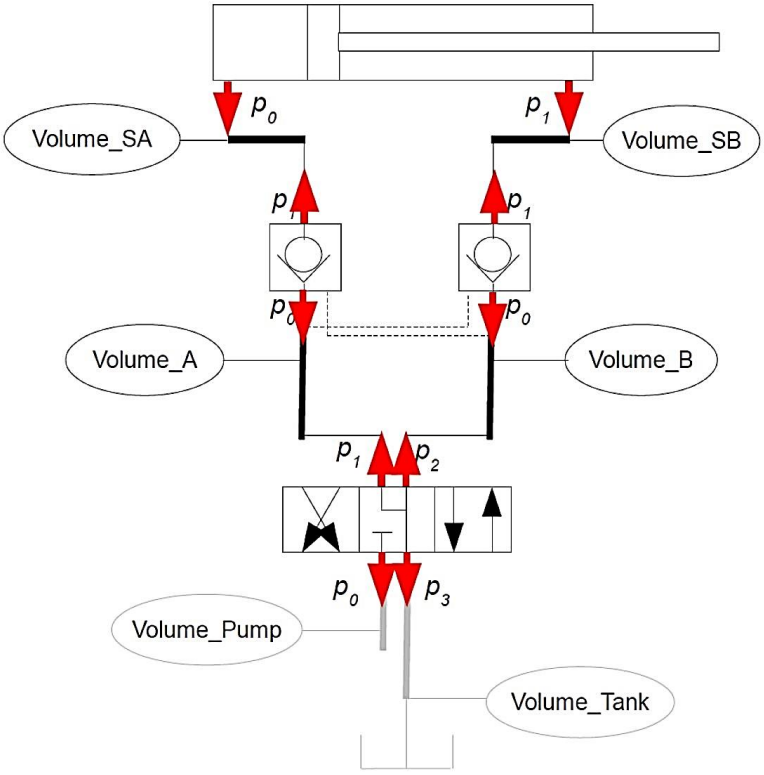

Figure 11. A basic hydraulic circuit divided into volumes (Korkealaakso 2015, p. 11).

The pressure in each volume is calculated as follows:

$$\dot{p}_i = \frac{B_{ei}}{V_i}\left(Q_{i,i} - Q_{o,i} - \dot{V}_i\right) \tag{11}$$

where $\dot{p}_i$ is the change of pressure of volume *i* with respect to time, B_{ei} is the effective bulk modulus of the fluid (including dissolved air) and its container, V_i is the capacity of volume *i*, $Q_{i,i}$ and $Q_{o,i}$ are the flow rates in and out of volume *I*, and $\dot{V}_i$ is the change of capacity in volume *i* with respect to time. (Watton 1989, p. 98.)

Furthermore, the volume flow through a valve is solved by using equation of turbulent flow (Korkealaakso 2015, p. 11) as follows:

$$Q = C_v a \sqrt{\frac{2(p_0 - p_1)}{\rho}} \tag{12}$$

where C_v is the flow coefficient, a is the area of flow, ρ is the density of the fluid, and $p_0 - p_1$ is the pressure difference across the component. The flow coefficient C_v is dependent on the type of valve and characteristics of flow. Therefore, it must either be defined experimentally, or like in most cases, acquired from a manufacturers data sheet. (Watton 1989, p. 35.)

The hydraulic cylinders play a large role in excavator simulation. In total, the simulation model includes 8 hydraulically actuated cylinders. The force produced by a hydraulic cylinder is created by the pressure of oil acting on the piston surfaces (Figure 12), and can be calculated by utilising equation 11 and the known piston areas as follows:

$$F = p_1 A_p - p_2 A_r - F_\mu \tag{13}$$

where F is the piston force, p_1 and p_2 are the cylinder pressures on the piston side and rod-side respectively, A_p and A_r are the piston area and rod-side area respectively, and F_μ is the friction force between the piston and the cylinder wall. Furthermore, the movement speed of the piston can be written as:

$$v = \frac{Q_1 - Q_L}{A_p} = \frac{Q_2 - Q_L}{A_r} \tag{14}$$

where *v* is the piston speed, Q_1 and Q_2 are, respectively, the volume flows to the piston side and the rod-side of the cylinder, and Q_L is the internal leakage flow rate. (Rabie 2009, p. 251.) In this case, the piston speed is defined by the multibody model, which is used to calculate the volume flows, internal friction and the force produced by the cylinder.

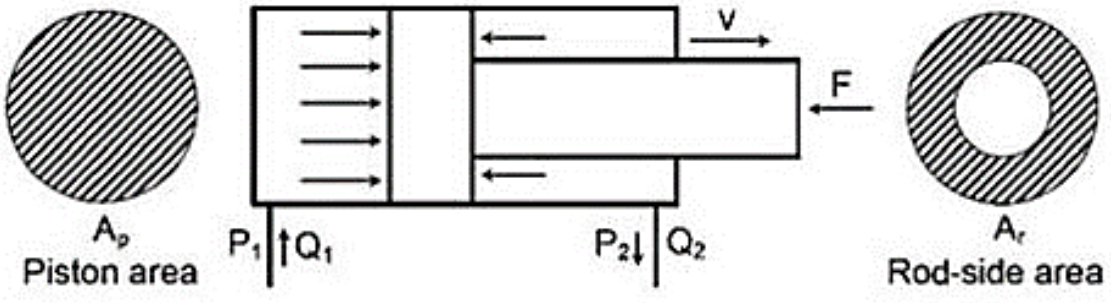

Figure 12. Schematic view of a double-acting hydraulic cylinder (Rabie 2009, p. 252).

3.4 Process modeling

One of the key factors in simulation of mobile working machines is the interaction between the environment and the machine. Called process modeling, it includes external elements such as hydraulic hoses, excavator tracks, and in earth moving operations different soil types like sand, clay and rocks. Correct process modeling serves two purposes. First, visually accurate environment can improve the operator experience and improve the effectiveness of training in simulation environment by providing realistic visual feedback to the trainee. In addition to providing nice visuals, the process model should also perform realistically. When an excavator is moved, the tracks will in most cases leave marks on the ground. Also, the material in the bucket will have certain weight affecting the excavator. Also during earth moving, the removed soil will leave a dent on the ground, and will pile up when dumped from the bucket. (Korkealaakso 2015, p. 15.)

As summarized by Korkealaakso (2015, p. 15), a realistically behaving environment model should include the following:

- "Sinking in the ground
- Soil compaction
- Embedding particles back to the soil with volume update, i.e. accumulation of material on the ground
- Visually and physically correct behaviour under operations like excavating, e.g. weight of the soil and soil resistance."

3.4.1 Soil model

Since mobile working machines often move on soil, and are used for moving various types of soil such as clay, sand and rocks, the simulation of soil behaviour is a key factor in real-time

simulation of excavators. To simulate ground behaviour realistically, Mevea employs an algorithm based on heightfield (also known as heightmap) technology, which allows accurate interaction between the terrain and the vehicle. Heightfields are widely used in creating virtual terrain. The height data is saved in a greyscale image as seen in Figure 13, where each pixel is given a value between 0 and 255 so that 0 is black and 255 white. By assigning the lowest height to value 0, and the highest to 255, one creates an image containing height data for the terrain. One advantage of using heightfields is the ability to create smooth ground by simply utilizing a blur filter on the created heightfield image. (Baros 2006, p. 51.)

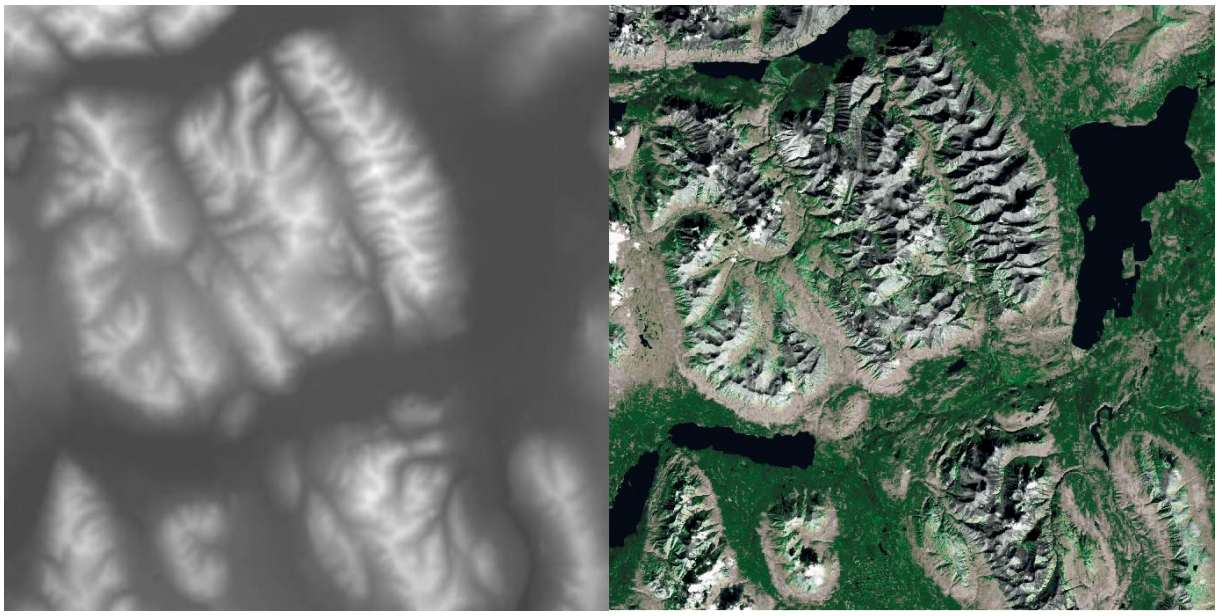

Figure 13. From left: A heightfield image (OpenTerrain 2011a) created from satellite imagery of Yukon, Canada. (OpenTerrain 2011b).

For Mevea, heightfield based approach offers features like machine sinking into the ground, soil compaction due to machine interaction, and both visually and physically accurate marking of the terrain by the machine. Furthermore, earth moving applications benefit from the ability to correctly simulate the mass of the soil in the bucket while loading, and at the unloading stage from the capability to embed the moved soil back to the terrain, while at the same time updating the heightfield properties. (Korkealaakso 2015, p. 20.)

3.4.2 Collision model

The modeling of collisions is an important aspect of real-time simulation. It is simulating the contact between the bucket and the sewer pipe in a realistic manner that is enabling the work

done on object detection in this thesis. Mevea utilises a triangularized collision model (Korkealaakso 2015, p. 16), which simply put means using triangularized geometries for both collision detection as well as collision response. To make the collision detection run smoothly during real-time simulation, a tree hierarchy is used as seen in Figure 14. At trunk and branch level oriented bounding boxes (OBB) are used, whereas the actual triangular collision only occurs at the primitive level.

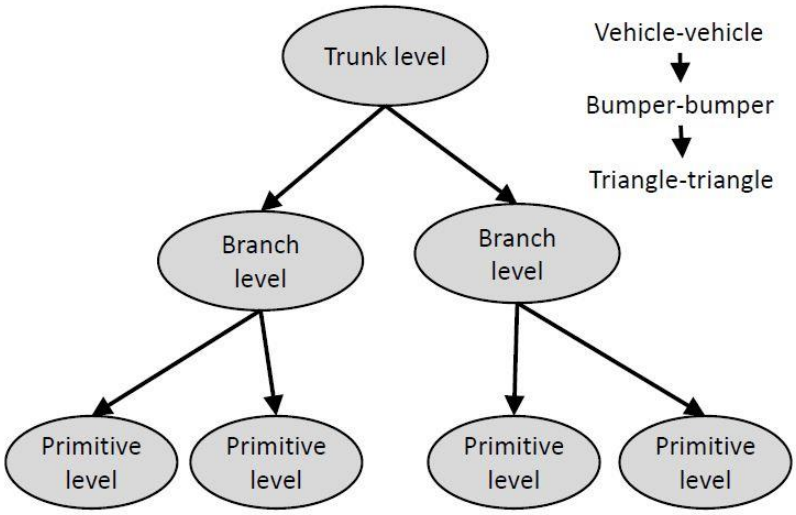

Figure 14. The tree shaped model used in collision detection (Moisio 2013, p. 21).

The use of OBB is necessary due to the otherwise labour intensive nature of collision detection. When using OBB representation, each component included in the collision simulation is given a virtual cube shaped volume (bounding box), which is tightly fitted around the extremities of the component and aligned with respect to the components local coordinate system, as opposed to being restricted to Cartesian coordinates. At the trunk level, the bounding box is usually assigned on large entities in the simulation environment, such as buildings or whole vehicles. Branch level includes individual components, such as an excavator bucket or individual teeth on the bucket. Collision checking occurs by determining when the geometries of the bounding boxes intersect with each other. Each time an intersection is detected, the collision detection moves to the next level of the collision detection tree. This procedure is continued until a collision happens and the primitive level is reached, or until intersection between the boxes is not detected, implying that a collision did not take place. Therefore, computation time is preserved as the primitive-primitive collision is only tested when necessary. (Coutinho 2013, pp. 29-31.)

The collision model in Mevea has a few significant advantages. First, the shape and geometry of the collision objects does not have any impact on the accuracy or functionality of the collision detection. Part meshing can be done without restriction on density or other properties. Even completely random orientation of triangles, so called polygon soup, will work. Also, dynamic friction is used instead of static fiction model, preventing the tendency of static objects to slide over time. To enable the use of a static friction model, temporal memory needs to be utilized. Temporal memory allows linking the previous states of the collision to the current collision event. This is achieved by assigning an id number for each triangle of the mesh, and tracking the collision history over different id numbers. (Moisio 2013, pp. 63-64)

3.5 Simulation model

As stated previously, the simulation model was run in Mevea Solver. The machine as well as the environment model used in this thesis were prebuilt by Mevea. In the simulation model, the excavator is placed on an area surfaced with sand (Figure 15).

Figure 15. Excavator model in the real-time simulation environment of Mevea Solver.

The modelled excavator is of generic type, although its design is based on a common real-world excavator. The model consists of several mechanical bodies as well as dummies, which is what bodies not connected to the kinematics chain are called in Mevea environment. Included in the system is also a complete hydraulic system model, including interaction with the internal

combustion engine used to power the hydraulic circuit. Table 2 presents a summary of the components included in the simulation model.

Table 2. Properties of the excavator simulation model (Mod. Korkealaakso 2015, p. 13).

Property	Value
Mechanical bodies	13
Dummy bodies	20
Valves	Pressure relief: 11 Counter balance: 3 Directional: 12 Safety: 15
Actuators	Cylinders: 8 Motors: 4 Pumps: 2
Hydraulic volumes	48
Simulation time step	1 ms
Control signals	25

The sewer pipe was added into the proximity of the excavator as a dummy part, and buried under the sand so that the pipe is completely hidden underground. Collision graphics were created directly from the same file as the visual pipe component. The collision properties were defined through trial and error method, by visually examining the behaviour of the collision in the simulation model. The defined properties between the pipe and the excavator bucket are presented in table 3.

Table 3. Collision properties between the excavator bucket and the dummy pipe as defined in Mevea Modeller.

Property	Value
Spring constant	1e8
Restitution coefficient	0.01
Damping coefficient	1e4
Velocity dependent stiffness	0
Friction coefficient	0.2
Normal direction	Body B (Bucket)
Use Friction	Yes

4 BUILDING THE STUDIED MODEL

4.1 Object detection

Several methods for object detection were studied and considered. Main focus was put on defining the forces acting on the bucket, which could be used to determine the collision with an object embedded in the soil. As originally proposed by Alekseeva et al. (1985) and reused by Koivo et al. (1996) among several others, the reaction force produced by the soil on the bucket, parallel to the digging direction, can be determined by:

$$F_r = k_p \left[k_s bh + \mu N + \varepsilon \left(1 + \frac{v_s}{v_b} \right) bh \sum_i \Delta x_i \right] \quad (15)$$

where k_p and k_s are specific cutting resistances for silty clay, b and h are, respectively, the width and thickness of the cut soil, μ is the friction coefficient between the excavator bucket and the soil, N is the pressure force applied by the bucket on the soil, ε is the resistance coefficient of the soil when filling the bucket, v_s and v_b are, respectively, the volumes of the dug soil and the bucket, and Δx_i is the horizontal increment in meters. (Koivo et al. 1996, p. 17.)

Also, an equation for defining digging forces named the "Fundamental Earthmoving Equation" (FEE) by Reece (1964) has seen wide usage in the field, including Luengo et al. (1998) and Kim et al. (2013). The FEE is written as:

$$F = \left(\gamma g d^2 N_\gamma + c d N_C + q d N_q \right) w \quad (16)$$

where F is the interaction force between the soil and the blade of the bucket, γ is the density of the soil, g is gravity, d is the depth of the bucket relative to soil, c is the soil cohesion, q is the vertical pressure from the bucket onto the surface of the soil, w is the width of the bucket, and N_γ, N_C, and N_q are factors depending on frictional strength of the soil as well as the geometry of the bucket, and relative strength properties of the bucket and the soil. (Luengo et al. 1998, p. 1901.)

As can be noted from the two equations, the different methods contain multiple variables difficult to define. Furthermore, the equations do not take hard objects into consideration, but assume the excavated soil to be homogenous. Although the variables could be found for one

simulation scenario, the accuracy in ever-changing conditions of real world applications is questionable. Without considering various soil types, the change of temperature or humidity can dramatically change the properties of even one type of soil. In addition, different excavator tools are used depending on the earth moving scenario, which again will affect the outcome of equations (15) and (16). Therefore, efforts were directed into determining the digging forces via the kinematic chain of the excavator arm, and the hydraulic cylinders used to actuate each link.

One criteria set for the object detection during digging, was the viability to move the simulated system from the simulation environment into a real-world scenario. Thus, while it would be possible to implement detection of hidden objects in the simulation environment by, for example, utilizing the built-in collision detection in Mevea Solver, such system could not be applied to a physical excavator with reasonable effort. The method proposed in this thesis is possible to implement in various ways, for example by using angle sensors in the joints between the excavator links, or by installing an inclinometer on each of the links. Since most of the digging work is done either by the hydraulic cylinder actuating the bucket or the arm, the system was set to detect sudden change of hydraulic pressure in these cylinders. This can be achieved by using force measuring pins to attach the cylinders, or by measuring the pressure of the hydraulic fluid acting on the piston by using pressure transducers. In the simulation environment, the cylinder forces used for object detection are obtained from data sources provided by Mevea Solver.

To determine the actual load on the excavator produced by digging, the load induced by the mass of the excavator components themselves need to be accounted for. The method presented here is based on the work by Koivo et al. (1996), and Cannon (1999). Since the geometry between the excavator links is changing during excavation, the equations need to take movement into consideration. In order to formulate the equations, important points such as joints and centers of mass in the excavator are assigned their individual letter, and angles between the links and actuators are defined according to Figure 16. (Koivo et al. 1996, p. 10.)

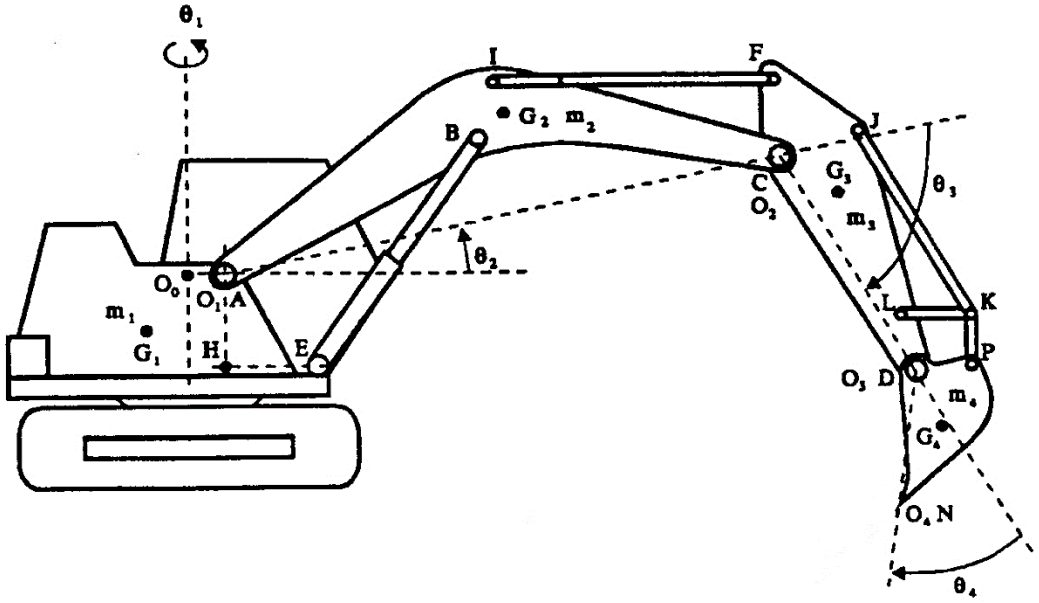

Figure 16. Schematic side view of the excavator showing the assigned joint angles and points (mod. Koivo et al. 1996, p. 11).

The location of the points is described by defining a Cartesian coordinate system for each link, and one fixed Cartesian coordinate system with its origin in the excavator body as shown in Figure 17. As can be noted from the figure, the rotation about the first coordinate system is vertical, while the other joints rotate around horizontal axis. However, it is assumed that during digging the excavator will only operate on one plane formed links O_1, O_2 and O_3. Therefore, it can be stated that $\theta_1 = 0$. (Koivo et al. 1996, p. 10.)

The equations describing the torque by gravity forces are formulated by applying Newton-Euler equations of motion for each link. Beginning from the bucket, the torque produced by the gravity force can be written as:

$$G_4 = -m_4 g L_{O3G4} \cos(\theta_{234} + \sigma_4) \tag{17}$$

where G_4 is the gravitational force affecting the bucket, m_4 is the mass of the bucket, g is gravity, L_{O3G4} is the distance between points O_3 and G_4, θ_{234} is the sum of angles θ_2, θ_3 and θ_4, and σ_4 is the angle between the points G_4, O_3 and O_4.

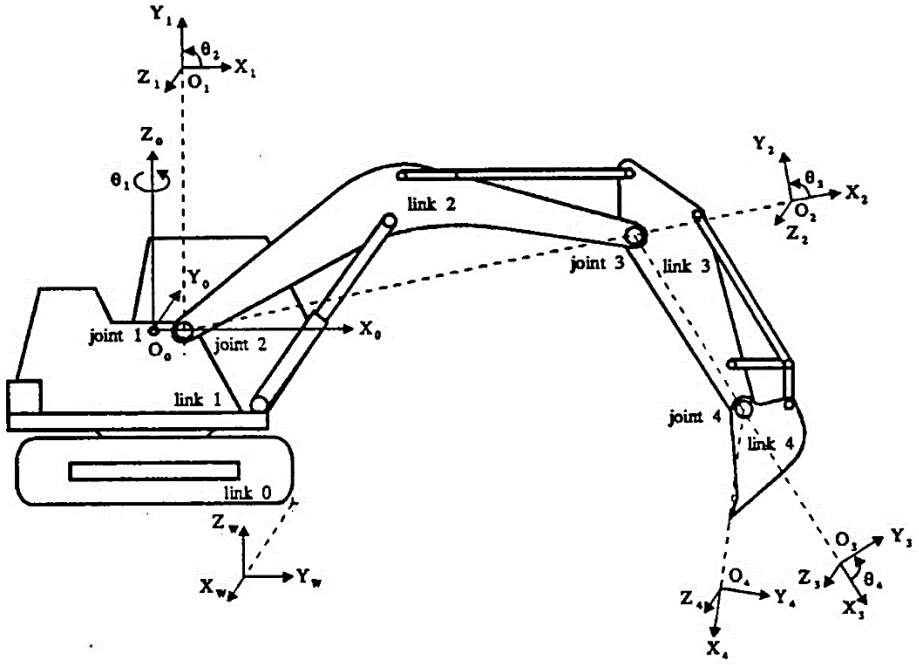

Figure 17. Cartesian coordinate systems assigned for each link and the body of the excavator (Koivo et al. 1996, p. 11).

The torque due to gravity force of the excavator arm can be written as follows:

$$G_3 = -m_4 g[l_3 c_{23} + L_{O3G4}\cos(\theta_{234} + \sigma_4)] - m_3 g L_{O2G3}\cos(\theta_{23} + \sigma_5) \qquad (18)$$

where G_3 is the gravitational force affecting the dipper arm, l_3 is the length between points O_2 and O_3, c_{23} is $\cos(\theta_2 + \theta_3)$, m_3 is the mass of the arm, L_{O2G3} is the distance between points O_2 and G_3, σ_5 is the angle between the points G_3, O_2 and O_3. (Koivo et al. 1996, p. 13.)

Besides gravitational forces affecting the joints, the hydraulic actuators produce linear force, which applies torque on the corresponding joints. In the proposed system, the torque is calculated for the dipper arm joint as well as the bucket joint, using a method described by Cannon (1999). For the dipper arm joint, the equation is as follows:

$$\tau_3 = F_3 a_3 \sqrt{1 - \left(\frac{b_3^2 - L_3^2 - a_3^2}{2 L_3 a_3}\right)^2} \qquad (19)$$

where F_3 is the force produced by the dipper arm cylinder, a_3 is the distance between points F and O_2, b_3 is the distance between points I and O_2, and L_3 is the length of the dipper arm cylinder which can either be determined by equipping the hydraulic actuator with a position

sensor, or calculated from the angle θ_3. The calculation of torque on the bucket joint is not as straightforward as it is for the dipper arm joint since the hydraulic actuator is connected to the bucket via link mechanism (Figure 18). The torque equation for the bucket joint is written as:

$$\tau_4 = \frac{F_4(e_1 \sin\gamma_3)}{\cos(\gamma_1+\gamma_2)-\sin(\gamma_1+\gamma_2)\cot\gamma_1} \tag{20}$$

where F_4 is the force produced by the bucket cylinder, e_1 is the distance between points O_3 and P.

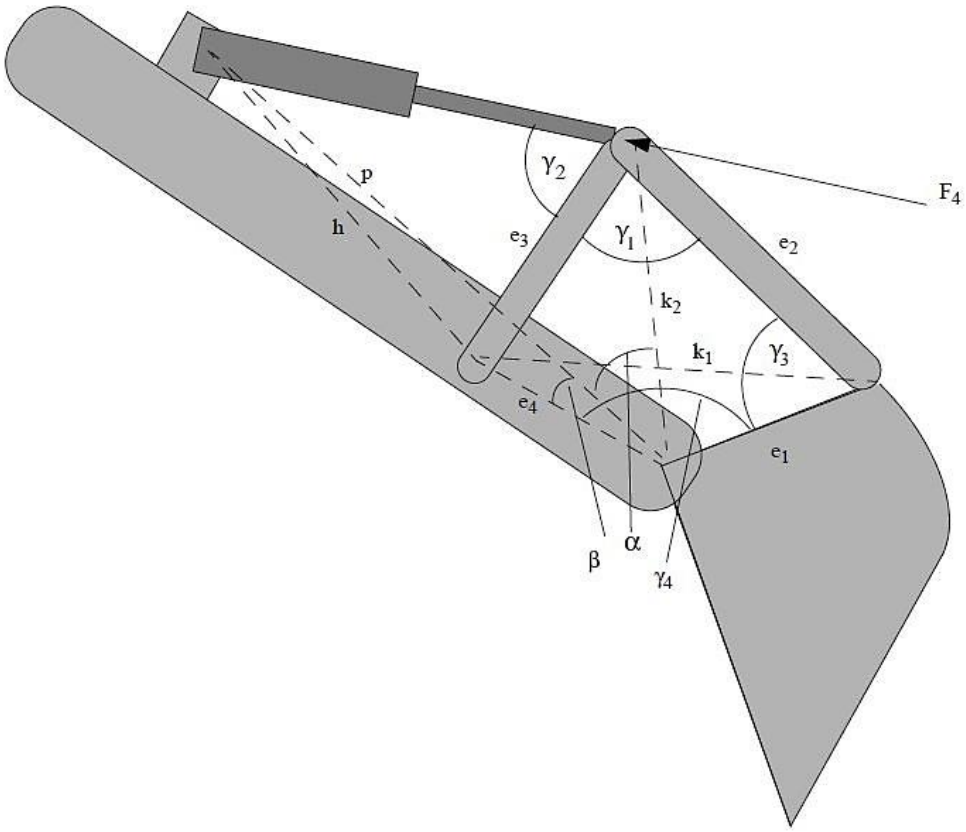

Figure 18. A simplified view of the bucket linkage. In order to avoid confusion with variables used by Koivo (1996), θ_1, θ_2 and θ_3 were changed to γ_1, γ_2 and γ_3 respectively. (Mod. Cannon 1999, p. 104.)

Furthermore, γ_1, γ_2 and γ_3 represent the angles ∠LKP, ∠JKL and ∠KPO_2 respectively. The angles in question are determined by utilising the knowledge of the bucket joint angle and law of cosines. First, the variable distance between points L and P is written as follows:

$$k_1 = \sqrt{e_4^2 + e_1^2 - 2e_4e_1\cos\gamma_4} \tag{21}$$

where e_1 and e_4 are the lengths of corresponding links, and γ_4 is the bucket joint angle. Next, angle γ_1 is defined by:

$$\gamma_1 = \cos^{-1}\left(\frac{e_3^2+e_2^2-k_1^2}{2e_3e_2}\right) \tag{22}$$

where e_2 and e_3 are the lengths of corresponding links, and k_1 is the distance between points L and P. Additionally, angle γ_3 is defined as

$$\gamma_3 = \cos^{-1}\left(\frac{e_2^2+k_1^2-e_3^2}{2e_2k_1}\right) + \cos^{-1}\left(\frac{e_1^2+k_1^2-e_4^2}{2e_1k_1}\right). \tag{23}$$

When the angles have been defined, the length k_2 between points K and O_3 can be written as follows:

$$k_2 = \sqrt{e_1^2 + e_2^2 - 2e_1e_2\cos\gamma_3} \tag{24}$$

To determine L_4, which is the length of the hydraulic cylinder actuating the bucket, angle α ($\angle JO_3K$) is calculated utilising the following equation:

$$\alpha = \cos^{-1}\left(\frac{e_4^2+k_2^2-e_3^2}{2e_4k_2}\right) - \beta \tag{25}$$

where β is a constant angle defined by $\angle LO_3J$. Now the equation for bucket actuator length can be written as:

$$L_4 = \sqrt{k_2^2 + L_{JO3}^2 - 2k_2L_{JO3}\cos\alpha} \tag{26}$$

where L_{JO3} is the length between points J and O_3. Finally, angle γ_2 can be written as:

$$\gamma_2 = \cos^{-1}\left(\frac{L_4^2+e_3^2-h^2}{2e_3L_4}\right) \tag{27}$$

where *h* is the constant length between points J and L.

Once the torques produced by the hydraulic actuators are known, the soil-tool interaction can be calculated by subtracting the torques due to gravitation force (G_3 and G_4) from the actuator torques. The constants used in calculation are presented in appendix 1.

4.2 Simulink model

The Simulink model was built using MATLAB version R2014b. The interface between Simulink and Mevea was preprogrammed by Jarkko Nokka. It allows the user to gain access to values of any data source in Mevea, while also enabling data input from Simulink back to Mevea. The outputs and inputs used in the Simulink model are listed in Table 4.

Table 4. I/O-signals connected to the Simulink model.

Inputs (from Mevea)	**Outputs (to Mevea)**
Joint angles: – Boom ($\boldsymbol{\theta}_2$) – Dipper ($\boldsymbol{\theta}_3$) – Bucket ($\boldsymbol{\theta}_4$)	Collision signal for joystick (0 or 1)
Actuator forces: – Dipper ($\mathbf{F}_3$) – Bucket ($\mathbf{F}_4$)	

The outputs in Mevea were defined by creating virtual angle sensors for joints O_1, O_2 and O_3. The readings of these sensors could then be defined as data sources, which are used as outputs to Simulink. Additionally, data sources were created from the forces produced by the hydraulic actuators. The force value is precalculated in Mevea Solver, and is the total sum of forces affecting the hydraulic actuator.

Figure 19 offers a schematic view of the model built in Simulink, where the initial step in object detection is taken by utilising the values input from Mevea, as well as constants presented previously. As stated earlier, the total torque on the joint is the sum of torque created by the hydraulic actuators and the gravitational forces. First, the torque by gravity on the dipper and the bucket joint was calculated along with the torques produced by the hydraulic actuators. Calculation was implemented per the equations presented in the previous chapter.

After the total joint torques have been summed, both torque signals were input into a discrete finite impulse response (FIR) filter to clear larger disturbances from the signals. The need for signal filtration became obvious during the initial testing of the system, when large spikes were created in the signal, mainly due to sudden changes in movement speed. Such situations occurred for example when the bucket or the dipper was rapidly moved back and forth by the operator, as in to shake the bucket empty of remaining soil. Thus, the system would return unwanted haptic feedback to the operator. In addition, the filter removes the signal spikes occurring as the hydraulic actuators reached the end of their travel. In theory, this could have been used to alert the operator of reaching the limit of cylinder travel, but was considered unnecessary at this point. It was also noted that if such a feedback were to be implemented, it would be less complex to implement using calculations based on the link angles or alternatively position transducers integrated into the hydraulic cylinders.

When digging in homogenous or nearly homogenous soil, the excavator arm moves at practically constant speed. Therefore, also the joint torques remain close to constant, and large changes only occur when facing an obstacle. The actual object detection was realised by taking a derivative of the filtered torque signals, thus resulting in a signal representing the rate of change of torque. The limit value for object detection was set by using the method of trial and error. The signal was observed during digging operations conducted in the real-time simulation environment. Excavation was done in homogenous soil so that the bucket moved freely across the whole digging motion, as well as so that the bucket encountered the pipe embedded in the terrain. The signal values were then compared so that the limit for collision signal output is high enough to not be triggered by unobstructed digging. Additionally, the limit was set as low as possible to trigger the operator feedback as soon as possible, enhancing the time given to the operator to react and avoid damage.

Finally, a simple if-condition was created to transform the rate of change signal into either 0 or 1. When the torque derivative exceeds the preset limit value, the system outputs 1, otherwise the output is 0. As the system monitors the condition of both dipper and the bucket joint separately, the output signals are merged so that the final output of the system is 1 if one or both limit values are exceeded, and 0 otherwise. The merged signal is then fed back into Mevea as a single output to initialize the vibration signal for the joystick.

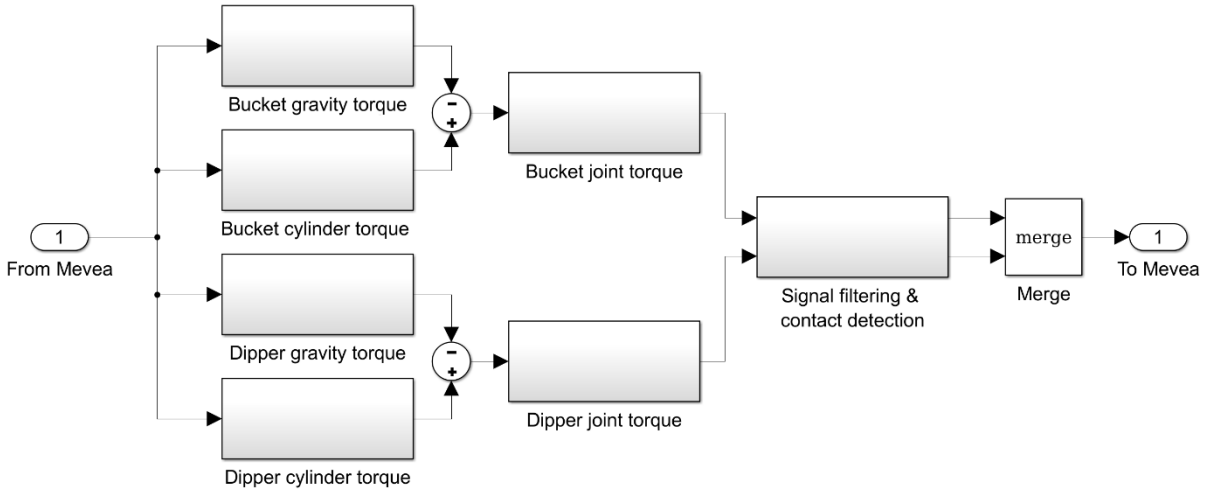

Figure 19. Schematic diagram of the model created in Simulink.

4.3 Considerations for teleoperation

Although this study mainly focuses on haptic feedback, the main source of operator feedback during teleoperation will still be visual feedback via video feed. Thus, consideration was given to the way in which visual feedback is presented to the operator. This includes aspects such as camera placement, viewing angle, and camera movement, which were defined based on previous research as well as practical testing of the setup.

The following criteria for camera placement were identified:

- operator should have close view of the bucket and the digging zone
- operator should be aware of the surrounding area
- operator should be able to recognize the position and orientation of the machine
- operator should be aware of the location of machine extremities
- camera placement and orientation should require minimal operator effort

Mevea Modeller allows versatile options for setting up multiple cameras in various positions, orientations and field of views. The orientation of the camera can either be set to be fixed, or to follow the movement of a specific body or an object in the world. The number of cameras is, in theory, unlimited, but for the sake of representing a real world remote control station the number of cameras was limited to 6. The use of remote observer robots proposed by Yu, Liu & Hasan (2010) were abandoned in order to keep the system as well as the user experience at a

simple and efficient level. By relying on cameras installed on the excavator alone, the operator needs to take care of a single vehicle and its controls, whereas with additional observer robots the operator focus and controls need to be occasionally shifted elsewhere. Moreover, the total cost of the system is reduced. As was discovered by Burks et al. (1994), a camera pointing towards the bucket and the digging zone turned out to be highly useful during digging trials. Therefore, a similar camera placement was adopted in the system studied in this thesis. The original design was improved upon by setting the camera to follow the movement of the bucket thus providing the operator with a constant and close view of the operation being conducted. Additional cameras were placed on the body of the excavator, two of which were equipped with a comparatively wide field of view and fixed orientation towards the excavator arm. These cameras give the operator a more general view of the digging area, with the possibility to observe the area from both left and right side of the arm. One fixed orientation camera was set high over the back of the excavator body, giving the operator the ability to see the whole excavator in one view. This camera position is intended to help the operator whenever maneuvering the excavator, in situations such as moving between different digging positions.

A camera system providing a 360-degree view suggested by Yu, Liu & Hasan (2010) was considered, but finally not adopted at this stage due to concerns related to available bandwidth and overcomplicating the overall system. The system would be beneficial for determining the extremities of the machine, thus possibly preventing collisions between the machine and the environment, especially when operating in confined locations. Such systems are already available on the market, and have been recently widely adopted by the automotive industry among others. Various system providers exist, but most of the systems operate in a relatively similar manner. For example, Continental produces a 360-degree camera systems equipped with 4 wide-angle cameras. The camera images can be processed to provide a top-down, 360-degree view of the vehicle, or they can be viewed individually depending on the situation. (Continental Automotive Systems, Inc. 2015)

Although the tested system is based on a conventional manned excavator, an excavator designed to be purely remote controlled would present different opportunities for the overall shape and design of the machine. The operator cabin could be completely removed creating space for mounting sensors or cameras for example, and in any case the design of the machine body could be simplified. Reduction in the size of the excavator body could potentially be exploited in

operation areas with constricted space, making it possible to operate inside buildings where a traditional excavator might not fit.

Depending on the technology used in teleoperation, signal delay might occur between the machine and the remote operator. Especially with wireless data transfer, the delay might be noticeably large. There might also arise issues such as signal corruption or, in the worst scenario, total loss of signal. The problems related to the connection between the machine and machine controls should be further investigated in further studies. From the point of haptic object sensing the delay in the data transfer should be kept as low as possible to avoid situations where object is detected, but the feedback to the operator isn't sufficient to react before damage is inflicted.

4.4 Measurements

Measurements of the system were conducted by utilising the signal logging system built into Simulink software. The data was gathered from 20000 data points, from every fifth timestep to keep the amount of data reasonable, while at the same time providing satisfactory accuracy. Data was gathered from a situation where the sewer pipe is completely hidden into the soil, and the bucket is moved on a trajectory resembling a typical digging scenario. The movement of the bucket and the arm was halted as soon as the operator noticed the object, either from the haptic feedback system, or visually from the movement of the excavator. Figure 20 and Figure **21** show the haptic feedback signal created from object detection, and the forces at the arm and the bucket cylinder created by the hydraulic actuators. In Figure 20, the haptic feedback system was turned off and the operator relied purely on visual feedback from the cameras, whereas in figure Figure **21** the operator was also provided with haptic feedback in addition to the camera system.

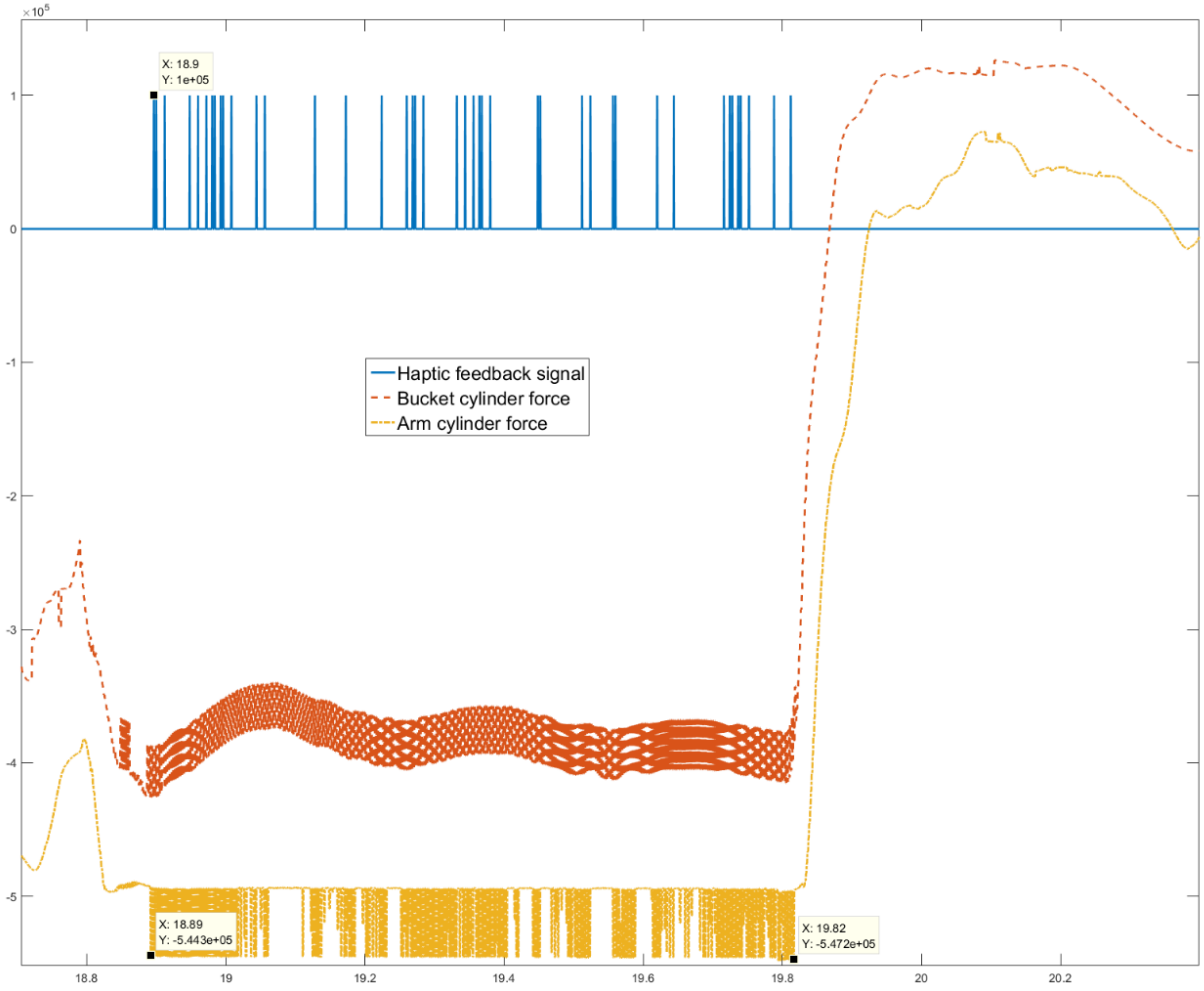

Figure 20. Graph presenting object detection signal (solid line), and the forces at the arm (dot-dash line) and bucket (dash line) cylinders during digging with the haptic feedback turned off.

With the haptic feedback turned off, the operator is able to detect the object and reverse the controls in 0,92 seconds from the object detection point. The reaction time was significantly decreased with the haptic system, as the cylinder force starts falling just after 0,35 seconds after the first object detection. Similar observations were made during practical testing of the system, where it was noted that without the haptic feedback system the collision can be detected only when the whole excavator begins to tilt. In a real-world scenario, similar forces would likely cause damage to pipes and ground wires and could also damage the excavator itself in the case of nonflexible object like a large rock. With the haptic feedback system engaged, the operator was able to react sooner thus limiting potential damages.

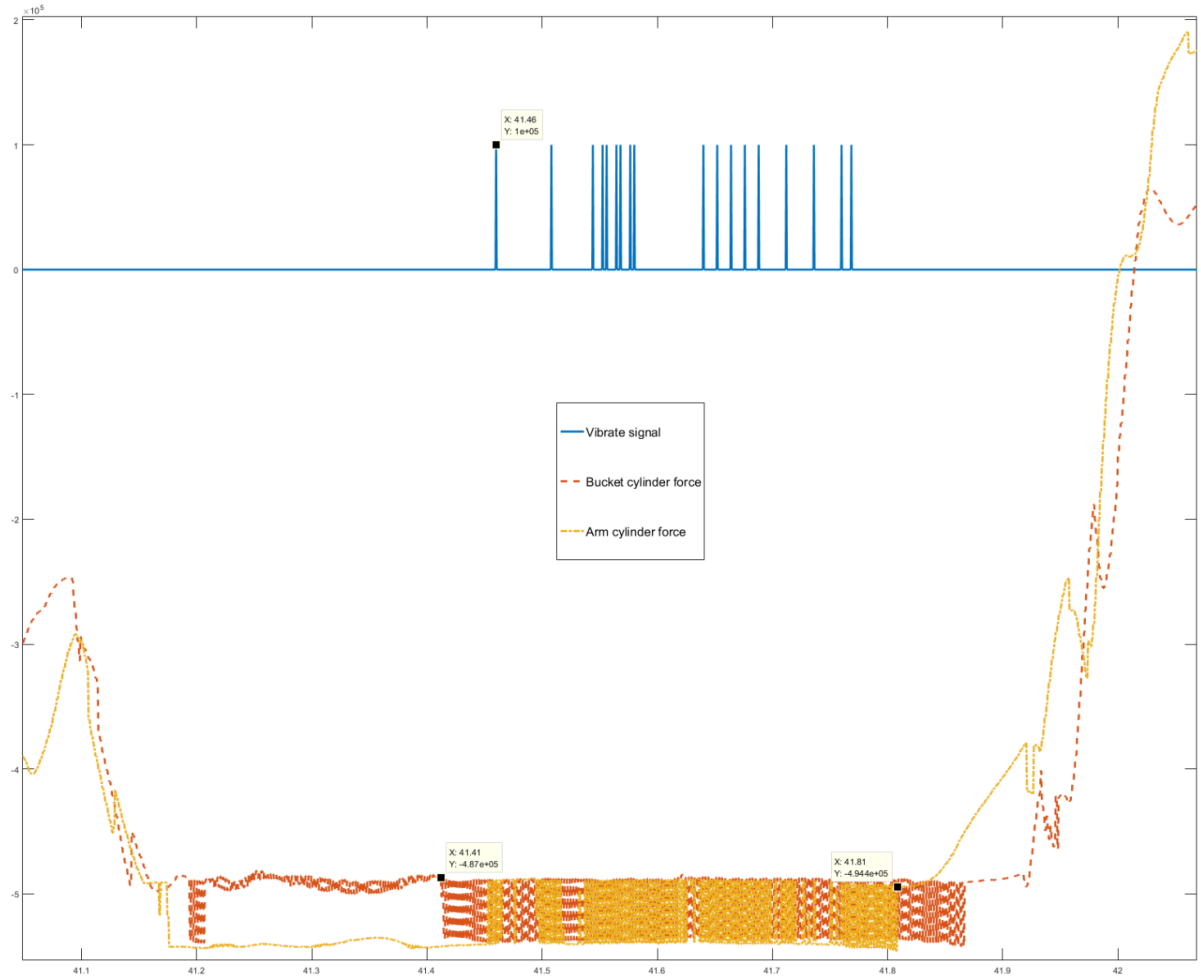

Figure 21. Graph presenting object detection signal, and the forces at the arm and bucket cylinders during digging with the haptic feedback turned on.

After the first user trials, it was noticed that the haptic feedback should be improved upon. The vibration signal created by the initial system produces a spiky signal as can be seen in figures 20 and 21. These spikes in the vibration signal also made the haptic feedback inconsistent making it difficult for the user to operate. In addition, the electric motor creating the vibration was occasionally unable to react fast enough to a single vibration signal pulse. This resulted in a situation where a collision was detected by the system, but the operator was unable to detect it via the haptic feedback. To remedy the issue, an off-delay switch was implemented (Figure 22) in the system. When a collision is detected and the vibrate signal changes from 0 to 1, the off-delay switch was set to keep the signal at 1 for 1.5 seconds. With this change, the user is provided with a 1.5 second pulse of vibration from the initial contact detection. Testing the system in practice resulted in a smoother and more consistent user experience. Additionally,

the off-delay switch ensures that the collision is detected instantly, from the first vibration signal spike.

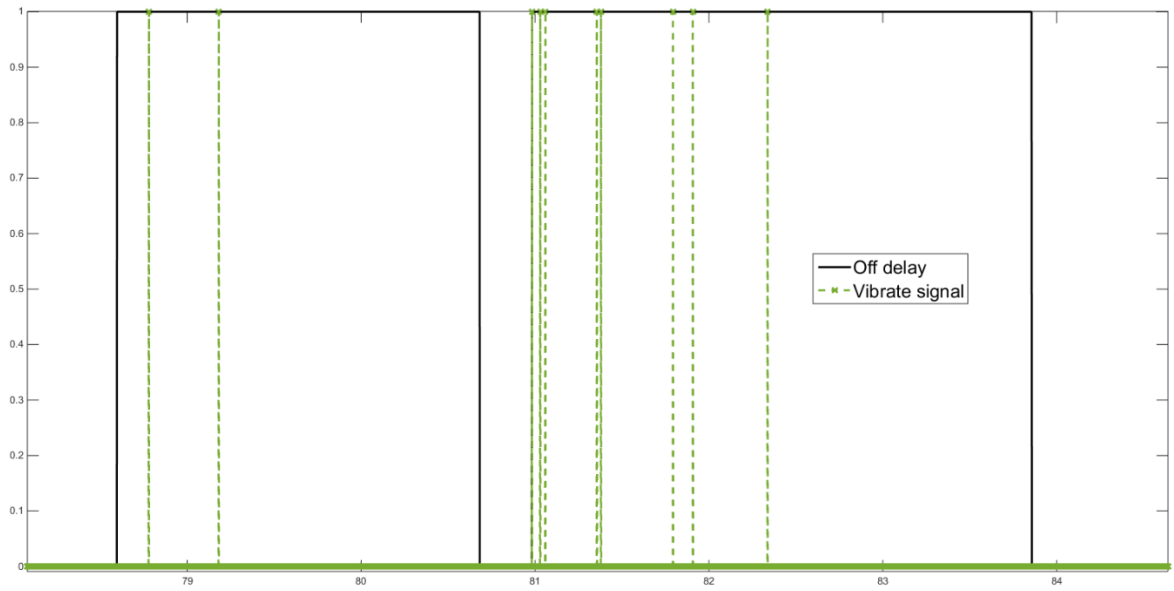

Figure 22. Graph displaying the function of the off-delay switch implemented on the vibration signal.

5 RESULTS & DISCUSSION

The aim of this work was to study previous research on haptic feedback and remote-control usage in the field of mobile working machines. In addition, the goal was to study the possible benefits of haptic feedback in excavator use by means of real-time simulation. During the study, a literature review was carried out, and a platform was created for evaluating the performance of haptic feedback in Mevea real-time simulation.

As a result of this study, a literature review was carried out, and a picture of the current state of haptic feedback system research in teleoperation was formed. The results of former studies suggest that some benefits could be achieved by implementation of haptic control system, which was also confirmed later in the experimental part of this study. Unlike the research done in this study, some of the previous work was done by studying 6DOF (6 degrees of freedom) joysticks such as the Phantom. Such devices are well suited for studies run in a laboratory environment, but present difficulties in real world usage. The space constraint for a joystick with multiple degrees of freedom is considerably larger than that of a traditional stick joystick. Moreover, the 6DOF joystick will completely alter the way in which the excavator is controlled, requiring even the experienced operators to undergo training with the new system. Furthermore, it was noted that the operator might become fatigued easier if one must struggle the haptic feedback constantly. Therefore, a haptic feedback system was built utilising a Simulink model for determining collisions between the excavator bucket and obstacles in the environment. The Simulink interface was connected to Mevea real-time simulation software. The haptic feedback system was completed by a Penny & Giles Ltd. JC6000 joystick with a generic electric vibration motor embedded inside the handle. Utilising this system, the operator isn't required to constantly counteract the haptic forces, but is instead only noticed of collisions via the vibrating stick.

The main benefits achieved with the studied system can be summed up as follows:

- decreased reaction time to collision with obstacles
- relatively straightforward implementation to real world applications
- relatively low cost of required equipment

The proposed camera system, which is a vital component in teleoperation, had both positive and negative results. The camera following the bucket movement provided a clear sight from proximity of the digging area, which made it possible to control the bucket in a more precise manner. The fisheye cameras on the sides of the excavator arm, however, were considered to distort the image to an extent where it became difficult to estimate the exact position of the arm. These cameras should be fitted with a narrower field of view lenses to achieve better operability, while the cameras mounted to the rear can still provide a wide-angle view of the excavator and its surroundings.

5.1 Future work

As the built control system will remain in an operable condition, it will allow for further development of the system itself, and can be utilised for additional studies on haptic control interface usage. Although the system is fully functional as it is, additional work is required to make the simulation model behave in a more realistic manner. This would include improving the model of the embedded object so that it would be flexible and not fixed in the ground. Furthermore, the simulation model should be experimented with different types of soil, since during this study only sand terrain was tested. The haptic control system could also be implemented and tested on different kinds of mobile working machines, such as wheel loaders, which operate in a similar manner to an excavator.

The issues related to network connectivity during teleoperation were not studied in this work due to the depth of the subject. Especially with wireless networks, the effect of network lag and other connection problems should be considered in future studies. The simulation of these effects proved to be troublesome during the literature review as the signal quality is defined by the surrounding environment thus creating numerous unknown variables. Nevertheless, some standalone software exists for simulating different types of networks which could be used in conjunction with Simulink.

Related to teleoperation, the camera system should also be studied in detail. The type of network utilized between the control station and the excavator will define the amount of available bandwidth, thus creating a constraint for the amount and quality of video streams. Additionally, the placement and viewing angles of the cameras should be improved upon, potentially with feedback from experienced excavator operators. Operating in dark conditions was not studied during this work, although ideally the machine should be able to operate during night time, as

well as in areas closed from sunlight. Using sufficient lighting, the usability window of normal cameras could be extended to cover low-light and dark conditions, although the image quality of the cameras in artificial lighting would require testing in real world conditions. Image intensifying cameras used in night vision devices for instance, could also be experimented on.

LIST OF REFERENCES

Alekseeva, T. V., Artemev, K. A., Bromberg, A. A., Voitsekhouskii, R. I. & Ulyanov, N. A. 1985. Machines for earthmoving work, theory and calculations. New Delhi, India: Amerind Publishing Co. 515 p.

Ban, Y. 2002. Unmanned Construction System: Present Status and Challenges. Proceedings of the 19th International Symposium on Automation and Robotics in Construction (ISARC). National Institute of Standards and Technology. Gaithersburg, Maryland, USA. 23-25.9.2002. Pp. 241-246.

Baros, M. 2006. Heightmap Terrain Rendering. Dr. Dobb's Journal, 31: 6. Pp. 51, 53-54.

Bayo, E., García de Jalón, J., Serna, M. A. 1988. A Modified Lagrangian Formulation for the Dynamic Analysis of Constrained Mechanical Systems. Computer Methods in Applied Mechanics and Engineering. 71: 2. Pp. 183-195.

Burks, B. L., Killough, S. M., Thompson, D. H. & Rossi, R. A. 1994. Telerobotic Excavation System for Unexploded Ordnance Retrieval. Twenty-Sixth DOD Explosives Safety Seminar. Miami, Florida. 16-18.08.1994. 19 p.

Cannon, H. N. 1999. Extended Earthmoving with an Autonomous Excavator. Master's Thesis, Robotics Institute, Carnegie Mellon University.

Cervin, A., Henriksson, D., Lincoln, B., Eker, J. & Årzén, K. 2003. How Does Control Timing Affect Performance? Analysis and Simulation of Timing Using Jitterbug and TrueTime. IEEE Control Systems Magazine. Vol. 23:3. June 2003. Pp. 16-30.

Continental Automotive Systems, Inc. 2015. 360 degree vehicle camera systems. [Continental Automotive Systems webpage]. [Referred 06.07.2017]. Available: https://www.vdo-instruments.com/camera-systems/360-degree-vehicle-camera-systems.html

Coutinho, M. G. 2013. Guide to Dynamic Simulations of Rigid Bodies and Particle Systems. London: Springer-Verlag. 399 p. Simulation Foundations, Methods and Applications.

Durfee, W., Sun, Z. & Van de Ven, J. 2015. Fluid Power System Dynamics. Center for Compact and Efficient Fluid Power. 54 p.

Hayashi, K. & Tamura, T. 2009. Teleoperation performance using excavator with tactile feedback. Proceedings of the 2009 IEEE International Conference on Mechatronics and Automation. Changchun, China. 9-12.8.2009. Pp. 2759-2764.

Hiramatsu, Y., Aono, T. & Nishio, M. 2002. Disaster restoration work for the eruption of Mt Usuzan using an unmanned construction system. Advanced Robotics. Vol. 16:6. Pp. 505-508.

Kim, Y. B., Ha, J., Kang, H., Kim, P. Y., Park, J. & Park, F.C. 2013. Dynamically optimal trajectories for earthmoving excavators. Automation in Construction. Vol. 35. November 2013. Pp. 568-578.

Koivo, A., Thoma, M., Kocaoglan, E. & Andrade-Cetto, J. 1996. Modeling and Control of Excavator Dynamics during Digging Operation. Journal of Aerospace Engineering. Vol. 9:1. January 1996. Pp. 10-18.

Korkealaakso, P. 2015. Real Time Simulation for Off-Road Vehicle Analysis [web document]. Madison, Wisconsin, USA: May 2015 [Referred 17.05.2016]. Presentation at Machine-Ground Interaction Consortium. University of Wisconsin Madison, Simulation-based engineering lab. 27 p. Available in PDF-file: http://sbel.wisc.edu/documents/Pasi_Presentation.pdf

Luengo, O., Singh, S. & Cannon, H. 1998. Modeling and Identification of Soil-tool Interaction in Automated Excavation. Proceedings of IEEE/RSJ International Conference on Intelligent Robotic Systems. Victoria, B.C., Canada. 13-17.10.1998. Innovations in Theory, Practice and Applications. Vol. 3. Pp. 1900-1906.

Mihelj, M. & Podobnik, J. 2012. Haptics for Virtual Reality and Teleoperation. Dordrecht: Springer Science+Business Media. 215 p. Intelligent Systems, Control and Automation: Science and Engineering 64.

Moisio, S. 2013. A Soft Contact Collision Method For Real-Time Simulation of Triangularized Geometries in Multibody Dynamics. Doctoral Thesis, Lappeenranta University of Technology, Lappeenranta.

OpenTerrain. 2011a. [Referred 30.05.2016]. Available: http://www.open-terrain.org/index.php/Keywords/HeightField

OpenTerrain. 2011b. [Referred 30.05.2016]. Available: http://www.open-terrain.org/index.php/Keywords/Imagery

Osafo-Yeboah, B., Elton, M., Jiang, X., Book, W. & Park, E. 2010. Usability Evaluation of a Coordinated Excavator Controller with Haptic Feedback. Proceedings of the 2010 Industrial Engineering Research Conference. Cancun, Mexico. Pp. 1-6.

Rabie, M. G. 2009. Fluid power engineering. New York: McGraw-Hill. 420 p.

Reece, A. R. 1964. The fundamental equation of earth-moving mechanics. Proceedings of the Institution of Mechanical Engineers. Conference Proceedings. Vol. 179:6. Pp. 16–22.

Rudus. 2017. EK-putket. [Rudus webpage]. [Referred 31.5.2017]. Available: http://www.rudus.fi/tuotteet/kaivot-ja-putket/ek-jarjestelma-kaivot-ja-putket/1623/ek-putket-pyoreat

Sakaida, Y., Chugo, D., Kawabata, K., Kaetsu, H. & Asama, H. 2006. The analysis of excavator operation by skillful operator. Proceedings of 23rd International Symposium on Automation and Robotics in Construction. 2006. Pp. 543–547.

Samur, E. 2012. Performance Metrics for Haptic Interfaces. London: Springer-Verlag London. 129 p.

Schmidt, D. & Karsten, B. 2010. An autonomous excavator for landscaping tasks. Proceedings for the joint conference of ISR 2010 and ROBOTIK 2010. Munich, Germany. 6-9.6.2010. VDI Düsseldorf. Pp. 819-826.

Shabana, A. A. 2010. Computational dynamics (3rd ed.). Chichester: Wiley. 528 p.

Shabana, A. A. 1998. Dynamics of multibody systems (2nd ed.). Cambridge: Cambridge University Press. 372 p.

Tavli, B. & Heinzelman, W. 2006. MOBILE AD HOC NETWORKS. Springer Netherlands. 265 p.

Watton, J. 1989. Fluid power systems: Modeling, simulation, analog and microcomputer control. New York: Prentice Hall. 490 p.

Yu, H., Liu, Y. & Hasan, M.S. 2010. Review of modelling and remote control for excavators, Int. J. Advanced Mechatronic Systems, Vol. 2: 1-2. Pp.68–80.

Yun-Joo, N. & Myeong-Kwan, P. 2015. Virtual excavator simulator featuring HILS and haptic joysticks. Journal of Mechanical Science and Technology, 29: 1. Pp. 397-407.

Yang, S., Jin, S. & Kwon, S. 2008. Remote control system of industrial field robot. 6th IEEE International Conference on Industrial Informatics 2008. Daejeon, South Korea. 2008. Pp. 442-447.

APPENDIX I

Constants used in the calculation of joint torques.

Constant	**Value [m]**
a_3	0.62616
b_3	2.4372
e_1	0.34
e_2	0.43151
e_3	0.51
e_4	0.27439
$\boldsymbol{h}$	2.09421
L_{JO3}	2.3662
L_{O3G4}	0.728
L_{O2G3}	0.8
l_3	2.30775
Constant	**Value [rad]**
$\boldsymbol{\sigma}_4$	0.52342
$\boldsymbol{\sigma}_5$	π
Constant	**Value [kg]**
m_3	794.96
m_4	750